

Design of an Automated Radio Telescope for Observing the 21 cm Hydrogen Line

A project report submitted in partial fulfillment of the
requirements for the degree of

Bachelor of Technology

by

Kshitij Duraphe-111805006

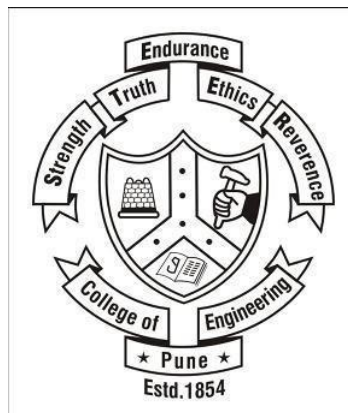
Revati Bhangale-111805071

Tanaya Wankhede-111705073

Divya Singh-111805074

Under the guidance of

Dr. S. S. Damhare
Dr. Archana G. Thosar



Electrical Engineering
COLLEGE OF ENGINEERING, PUNE
2021-22

Project Report Approval

The project report entitled

Design of an Automated Radio Telescope for observing the 21 cm Hydrogen Line

by

Kshitij Duraphe-111805006

Revati Bhangale-111805071

Tanaya Wankhede-111805073

Divya Singh-111805074

is approved for the degree of

Bachelor of Technology

of

Electrical Engineering Department

College of Engineering, Pune

Examiners	Name	Signature
1. External Examiner	_____	_____
2. Head of Department	_____	_____
3. Guide	_____	_____

Date:_____

Place:_____

COLLEGE OF ENGINEERING PUNE, INDIA


CERTIFICATE

This is to certify that project report entitled **Design of an Automated Radio Telescope for observing the 21 cm Hydrogen Line** submitted by **Kshitij Duraphe** (MIS-111805006), **Revati Bhangale** (MIS-111805071), **Tanaya Wankhede** (MIS-111805073) and **Divya Singh** (MIS-111805074) is a record of bonafide work carried out by them, under my guidance, at College of Engineering, Pune in partial fulfillment of the requirement for the award of the degree of **Bachelor of Technology in Electrical Engineering** from University of Pune.

Date:

Place:

Dr. Archana G. Thosar
Professor
Electrical Engineering
College of Engineering
Pune – 411005



Dr. S. S. Damhare
Head of Department
Electrical Engineering
College of Engineering
Pune – 411005

Abstract

Observing extraterrestrial radio emissions has become significantly easier due to the advance in electronic technology. The detection of emissions of neutral hydrogen from sources outside the solar system is a very achievable task for amateurs nowadays. Cheap and widely available radio components are the primary reason behind this. We probe the universe to find various sources of neutral hydrogen radiation, using a custom-designed horn antenna, ready-to-use electronic components such as low noise amplifiers and software-defined radios, and spectrometers.

Contents

Abstract	4
List of tables	7
List of Figures	8
Nomenclature	11
Abbreviations	12
1. Introduction, literature survey and problem statement	
1.1 Introduction.....	13
1.1.1 Strength of Radio Emissions.....	14
1.1.2 Basic Antenna Theory	14
1.1.3 Some common types of Antenna	16
1.1.4 Radio Telescopes	23
1.1.5 Amateur Radio Astronomy	24
1.2 Literature review	25
1.3 Motivation.....	27
1.4 Aims and Objectives.....	28
1.5 Problem statement.....	2
2. Horn Antenna	
2.1 Horn Antenna Design.....	31
2.2 Optimum Pyramidal Horn Design.....	36
2.3 Modified Horn Antenna Equation.....	37
2.4 Waveguide Design.....	39
2.5 Coaxial Transition Design.....	47

3. Results	
3.1 Simulation Results and comparison with other commercially viable Available Calculators.....	49
3.2 Atmospheric Attenuation.....	57
4. Hardware Setup	
4.1 Hardware Setup	59
5. Observations	
5.1 Spectrometric Software Observations	69
5.2 Our implementation of a scaled down form of Virgo.....	73
5.3 Calculations.....	75
6. Conclusion and future scope	
6.1 Conclusion.....	79
6.2 Future scope	79
6.3 Challenges	80
Bibliography	81
Acknowledgement	83
Appendix.....	84

List of Tables

Table.1: VSWR vs Reflected Power.....	52
Table.2: Specifications of RF Amplifier.....	65
Table.3: Readings for the galactic rotation curve	77

List of Figures

Fig.1: Loop Antenna Radiation Pattern	15
Fig.2: Dipole Antenna.....	17
Fig.3: Dipole Antenna Radiation Pattern.....	17
Fig.4: Corner Reflector Antenna.....	18
Fig.5: Corner Reflector Radiation Pattern	18
Fig.6: Turnstile Antenna	19
Fig.7: Turnstile Antenna Radiation Pattern	19
Fig.8: Monopole Antenna	20
Fig.9: Monopole Antenna Radiation Pattern	20
Fig.10: Yagi-Uda Antenna.....	21
Fig.11: Log-Periodic Dipole Antenna.....	21
Fig.12: Micro strip Antenna.....	21
Fig.13: Loop Antenna	22
Fig.14: Aperture Antenna	22
Fig.15: Aperture Antenna Radiation Pattern	23
Fig.16: Radio Telescope	24
Fig.17: H-plane and E-plane Horn Antenna	32
Fig.18: Rectangular Aperture with uniform electric field	32
Fig.19: H-plane Sectoral Horn.....	33
Fig.20: E-plane Sectoral Horn	35
Fig.21: Pyramidal Horn Antenna.....	35
Fig.22: Optimum Pyramidal Horn Antenna.....	36
Fig.23: Types of waveguides	39
Fig.24: Rectangular Waveguides.....	41
Fig.25: Waveguide Dimensions.....	48
Fig.26: Horn Antenna Design in Ansys HFSS	49

Fig.27: Horn Antenna Directivity in Ansys HFSS	50
Fig.28: Horn Antenna Radiation Pattern in Ansys HFSS.....	50
Fig.29: Simulated S11 pattern.....	51
Fig.30: VSWR through simulation	53
Fig.31: Smith Chart for S Parameter.....	53
Fig.32: Waveguide Antenna element.....	54
Fig.33: Performance of Pin Feed- Phase.....	54
Fig.34: Performance of Pin Feed- VSWR	55
Fig.35: Performance of Pin Feed- Return Loss	55
Fig.36: Simulation in MATLAB- Radiation Pattern	56
Fig. 37: Simulation in MATLAB- Return Loss.....	56
Fig. 38: Simulation in MATLAB- VSWR.....	57
Fig. 39: Ideal Atmospheric Attenuation at 1.42GHz over Pune.	58
Fig. 40: Realistic Atmospheric Attenuation at 1.42GHz around the world.	58
Fig. 41: Block Diagram of Professional Observatory.....	59
Fig. 42: Block Diagram of Super heterodyne Receiver.	60
Fig. 43: RTL-SDR.....	61
Fig. 44: Block Diagram of RTL-SDR (a).	62
Fig. 45: Block Diagram of RTL-SDR (b).	62
Fig. 46: RTL-SDR part labelling.	63
Fig. 47: Cascaded Amplifiers.....	64
Fig. 48: RF LNA.	65
Fig. 49: Fabricated Horn Antenna.....	66
Fig. 50: Fabricator's Dimensions of Horn Antenna.	67
Fig. 51: Antenna Feed, Connector, RTL-SDR.....	68
Fig. 52: 1.42GHz observation setup in SDR Sharp.	69
Fig. 53: 1.44GHz observation using SDR Sharp.	70
Fig. 54: SDR Artefacts recorded on SDR Sharp.....	71
Fig. 55: Readings obtained by Horn Antenna when it is not pointed to any source.	72

Fig. 56: Readings obtained by Horn Antenna when it is pointed to galactic center.	72
Fig. 57: HI Profile from the LAB survey of the galactic center.	74
Fig. 58: Galactic Center Position Prediction.....	75
Fig. 59: Galactic Rotation configuration.....	76
Fig.60: Initial plotting of Galactic Rotation Curve.	78
Fig. 61: Galactic Rotation Curve.....	78
Fig. 62: Stellarium's User Interface.	84

Nomenclature

α	Fine-structure constant
ΔE	Energy change
Z	Atomic number
m	Mass of the electron
M_n	Nuclear mass
c	Speed of light
g_n	Nuclear gyromagnetic ratio
n	Number of electrons
f	Number describing cumulative spin
λ	Wavelength
\hbar	Reduced Planck constant
B	Magnetic Field Strength/E-plane Horn Dimension
μ_0	Magnetic permeability
J	Electric current density
E	Electric field strength
ϵ_0	Electric permittivity
P_t, P_z	Poynting vector/Poynting vector in z-direction
Ω	Solid Angle
I	Current
dl	Line element
R_a	Characteristic impedance
a, b	Rectangular waveguide width and height
β_0	Waveguide propagation constant
X_k	DFT of the signal
$e^{-j\beta z}$	Attenuation factor
F	Noise figure
G	Gain, Gravitational Constant

Abbreviations

RF	Radio Frequency
SRT	Small Radio Telescope
SNR	Signal-to-Noise Ratio
SMA	Sub miniature Type A

Chapter 1

1.1 Introduction

A bound quantum system can only take on some discrete energy values called energy levels. Degenerate energy levels are energy levels that correspond to two or more different measurable states of a quantum system. Small shifts in degenerate energy levels occur due to multipole interaction between the nucleus of an atom and the surrounding electron cloud. The nuclear magnetic dipole moment interacts with the magnetic field of the electrons and the distribution of charge within the atom (giving rise to the electric quadrupole moment in the nucleus) leads to what is called a hyperfine structure of the atom. A single electron orbits a proton in a neutral hydrogen atom. The inherent magnetic dipole moments of the electron and the proton cause changes in the energy of the system due to their interaction. The energy change due to these interactions is given by:

$$\Delta E = \frac{2}{3}(Z\alpha)^4\left(\frac{m}{M_N}\right)(mc^2)g_N\frac{1}{n^3}\left(f(f+1) - \frac{3}{2}\right)$$

where f is simply the sum of the possible spins and α is the fine structure constant. Both the proton and an electron have a spin off $\pm\frac{1}{2}$ and therefore f can take on the values 0 and 1. This means that the energy difference for the hyperfine splitting is given by $\Delta E_{f=1} - \Delta E_{f=0}$.

Taking the value of the fine-structure constant as $\frac{1}{137}$, the transition energy is given by $\frac{4}{3}\left(\frac{1}{137}\right)^4\left(\frac{.51}{938}\right)(.51 * 10^{-6})(5.56) = 5.84 * 10^{-6}eV$. The wavelength of this emission,

therefore, is $\lambda = 2\pi\frac{\hbar c}{E} = 2\pi\frac{1973}{5.84 * 10^{-6}}\text{\AA} = 21.106cm$. The frequency corresponding to this wavelength is therefore $1420.405MHz$. The $f = 1$ state naturally occurs in interstellar neutral hydrogen clouds due to collisions between the hydrogen atoms, leading to photon emission at this specific frequency. These emissions can reach out into deep space because of the large value of the photon's mean free path in the cloud.

Due to the movement of these interstellar clouds relative to the observing stations on Earth, these emissions are recorded at Doppler-shifted frequencies. Analysis of these frequencies allows one to divine the relative velocities and arrangement of these structures. The uneven mass distribution of our galaxy results in different frequencies detected from different regions of space. To detect these emissions, we build a radio telescope in the form of a horn antenna with a custom waveguide and ready-to-use electronic components such as amplifiers.

1.1.1 The strength of Radio Emissions:

The inverse-square law is the most significant factor in determining the irradiance received by a ground observer from stellar sources. For example, the distance between the Sun and the galactic centre is about 8.5 kilo parsec (kpc), or approximately $2.6 * 10^{20}m$. This means that the power reaching the Earth from the galactic centre is 10^{-40} times the power emitted at 1m. Therefore, the actual energy reaching any radio telescope is extremely small and must be amplified many times for a functional reading. For example, the cooling temperature for hydrogen clouds is of the order of $100K$, which results in a power output of roughly $4 * 10^6W$ at a distance of $1m$ from the source by the Stefan-Boltzmann law. The power reaching the Earth is roughly of the order of $10^{-34}W$. Since the Stefan-Boltzmann law describes perfect black bodies (which the clouds cannot be), the value arrived at with this rough calculation is many orders of magnitude larger than the actual value. We use this to merely illustrate the scales which radio telescopes operate at.

1.1.2 Basic Antenna Theory:

There are two main types of communication systems: those that rely on energy propagation with physical connections, and those that rely on the electromagnetic spectrum using antennas to transmit and receive energy. An antenna is a structure, usually made from a good conducting material that has a specifically designed shape and size so that it radiates

electromagnetic power in an efficient manner. The equation $\nabla \times B = \mu_0 J + \mu_0 \epsilon_0 \frac{\partial E}{\partial t}$,

better known as the fourth Maxwell equation, shows how time-varying electric currents generate magnetic fields. An antenna is therefore a structure on which time-varying currents can be generated to produce electromagnetic radiation. This can be achieved when the antenna is connected to a suitable source by means of a waveguide.

It is also well-established that electromagnetic waves, upon impact with a conductor, create a potential difference that leads to minute currents being formed. These currents can be detected with a suitable detector; the transmission line or waveguide operates in reverse, allowing the antenna to act as a receiver. If the current density J on the surface of the antenna is known, then the calculation of the emitted electromagnetic field can be performed. Due to the linearity of Maxwell's equations, the antenna can be divided into small filaments of length dl with a current I passing through them; and if the radiation from these small current elements is known, the principle of superposition can be applied. This is the approach used by simulation software to determine the radiation of an antenna.

Some parameters that define the antenna are its radiation pattern, beam width, directivity, and radiation resistance. The radiation pattern can be defined as the relative distribution of radiated power as a function of direction in space.

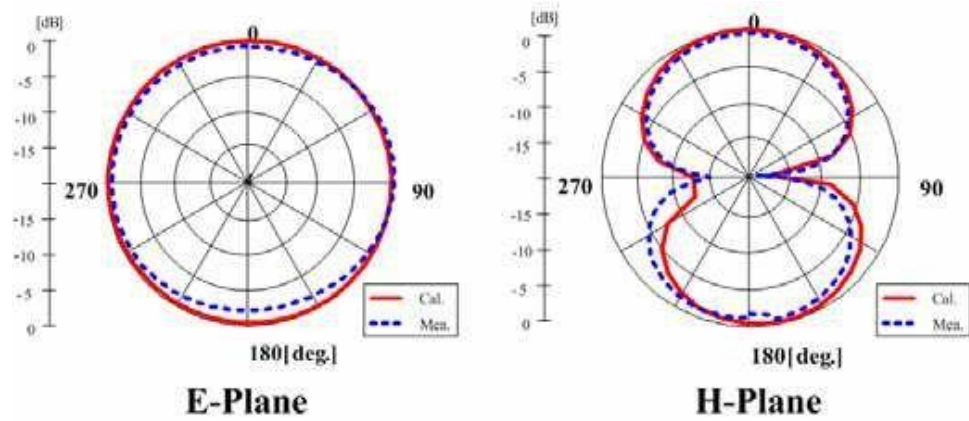


Fig. 1: Loop Antenna Radiation Pattern

The directivity, closely associated with the gain, is a measure of the intensity of radiation with respect to position in space. The intensity of radiation is simply the power per unit solid angle, and thus we can define it as the product of the Poynting vector flux density by the square of the distance. For the dipole, this is:

$$\frac{dP_t}{d\Omega} = \frac{r^2}{2} \text{Re}(E \times H) \cdot a_r$$

and hence the directivity can be defined as $4\pi \frac{dP_t/d\Omega}{P_t}$ where P_t is the total power radiated. We can integrate the Poynting vector power flux imagining that a closed spherical surface surrounds the dipole, which is equivalent to integrating the intensity over the solid angle of a sphere. Thus, the total power is:

$$P_t = \frac{dP_t}{d\Omega} \int_0^{2\pi} \int_0^\pi \sin^2\theta d\Omega$$

Using the above two equations, it is easily seen that $D(\theta, \phi) = 1.5\sin^2\theta$, which shows that the maximum value of directivity is 1.5. This means that the antenna would, at max, produce 1.5 times the maximum power in a direction that an isotropic radiator would produce.

Antennas can be essentially thought of as passive parts of a transmission line. Therefore, a quantity called the radiation resistance is important. In simple terms, the radiation resistance is the resistance that would dissipate the same amount of power an antenna does when the currents applied to the antenna and the resistance are the same. For a dipole antenna, using the

formula $\frac{1}{2}I^2R_a = P_r$, the integral when substituted results in $R_a = 80\pi^2\left(\frac{dl}{\lambda_0}\right)^2$.

1.1.3 Some common types of Antenna:

The most common type of antenna is the dipole antenna.



Fig. 2: Dipole Antenna

This antenna consists of two straight conductors arranged symmetrically, with the transmitter being attached to one conductor and the receiver attached to the other. The conductor length is often kept at a quarter of the wavelength it is meant to be used for. The radiation pattern of this antenna is strongest in directions perpendicular to the axis.

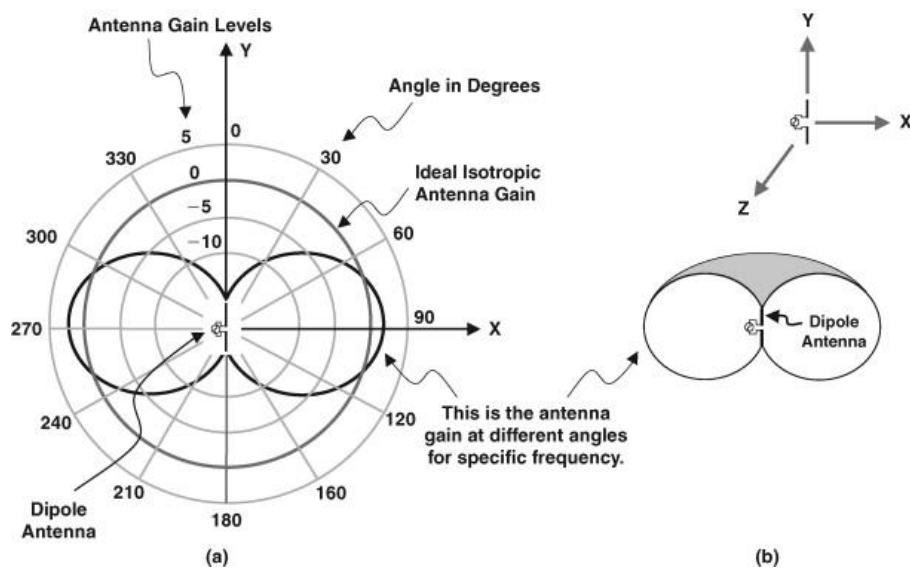


Fig. 3: Dipole Antenna Radiation Pattern

Some antennas, such as corner reflectors and turnstile antennas, are made using the quarter-wave dipole as a basis.



Fig. 4: Corner Reflector Antenna

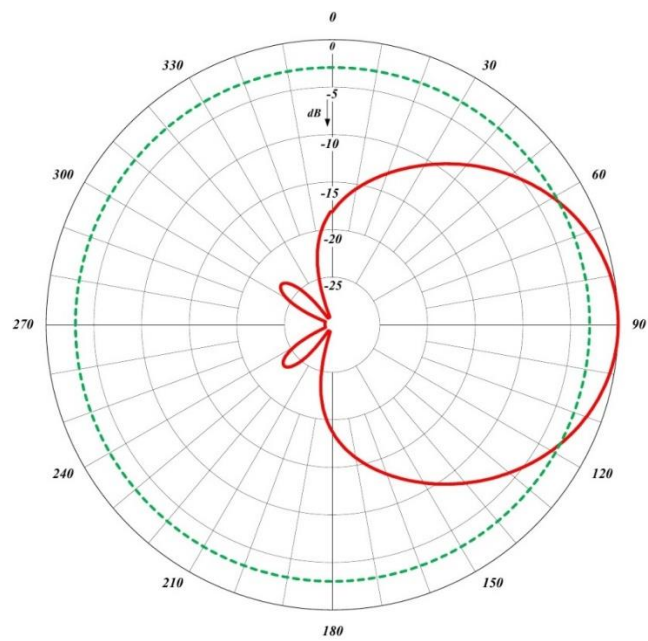


Fig. 5: Corner Reflector Antenna Radiation Pattern



Fig. 6: Turnstile Antenna

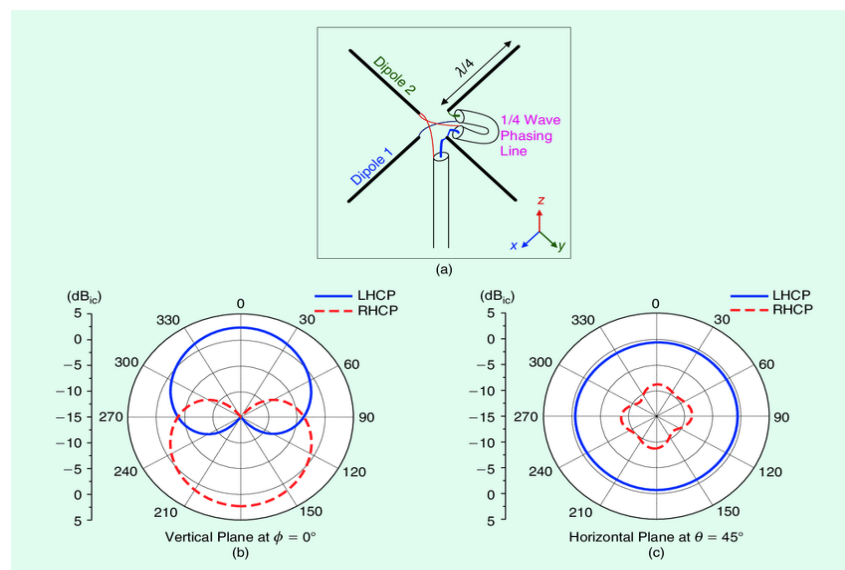


Fig. 7: Turnstile Antenna Radiation Pattern

Monopole antennas are single straight conductors attached to a reflecting surface called a ground plane. These types of antennas work using the concept of an image antenna.



Fig. 8: Monopole Antenna

The radiation pattern of a monopole antenna is the same as the radiation pattern of one conductor of a dipole antenna. Monopole antennas are commonly seen in cars, where they are used as radio receivers.

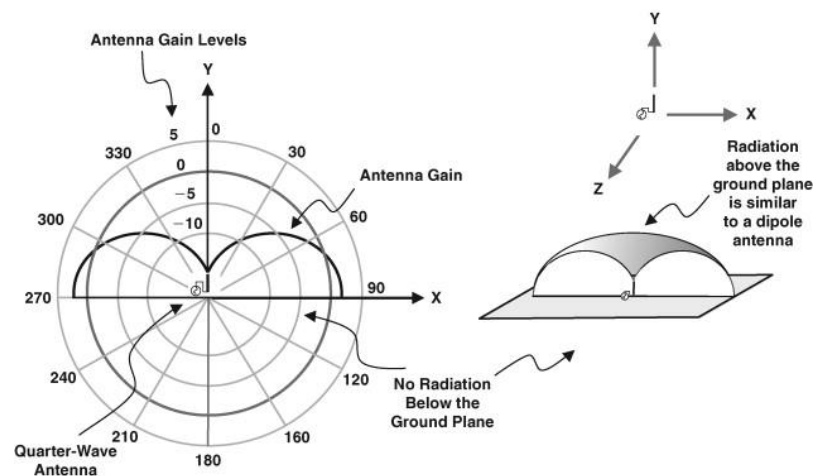


Fig. 9: Monopole Antenna Radiation Pattern

Antenna arrays usually consist of straight monopole antennas connected in different patterns. Some of these types of antennas include the Yagi-Uda antenna, the Log-periodic dipole antenna, and the micro strip antenna. These find many applications and are the most commonly used antennas in the world.

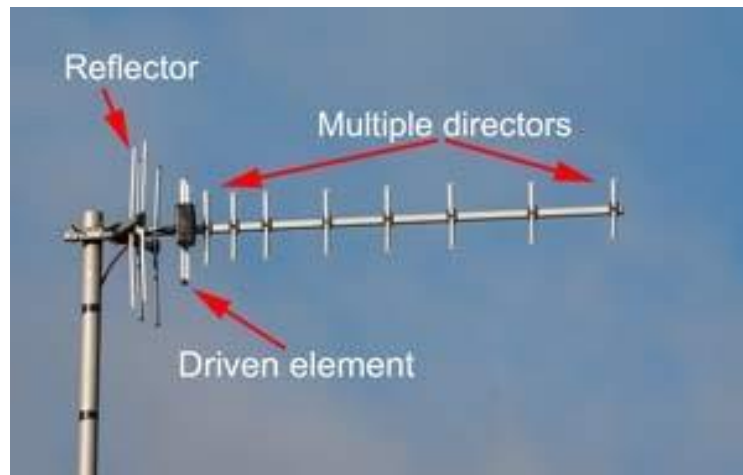


Fig. 10: Yagi Uda Antenna



Fig. 11: Log Periodic Dipole Antenna

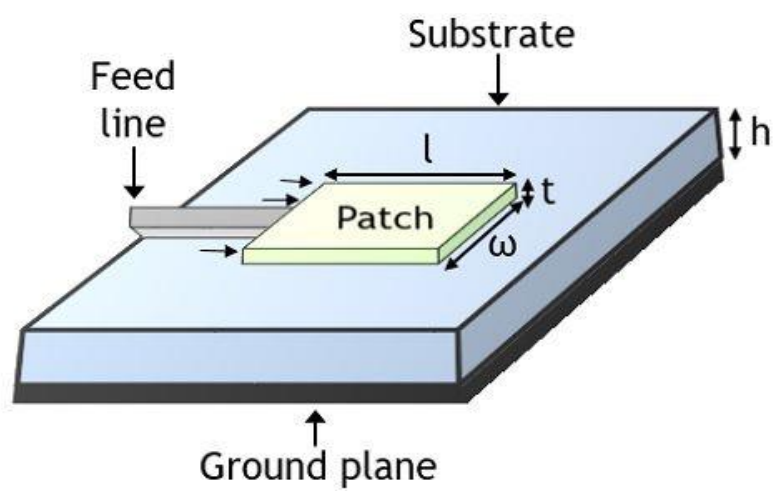


Fig. 12: Micro Strip Antenna

Loop antennas are coils of conductors that interact only with the magnetic component of the electromagnetic radiation. This means that they are generally not affected by electric noise. They generally have very high efficiency. The trade-off is high radiation resistance.



Fig. 13: Loop Antenna

The final type of antenna is the aperture antenna. Aperture antennas consist of antennas such as parabolic reflectors, horn antennas, slot antennas, and so on. These types of antennas are used for emitting or receiving radiation in a certain direction. The apertures act as ‘buckets’ to capture or emit radiation. They are generally very directional and very powerful.

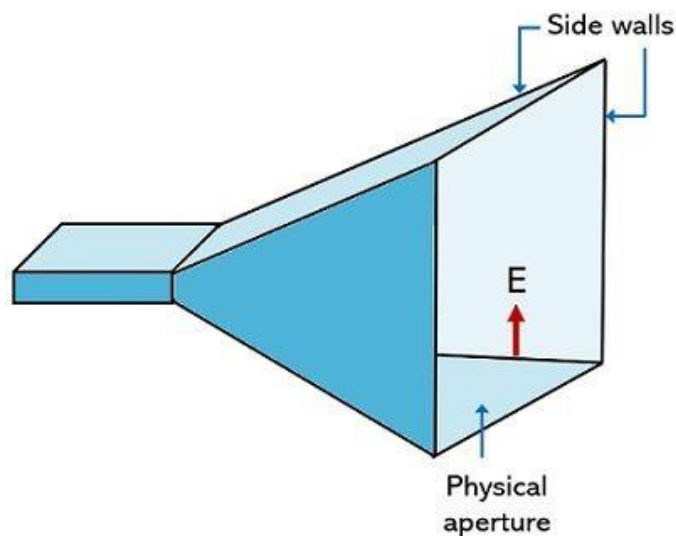


Fig. 14: Aperture Antenna

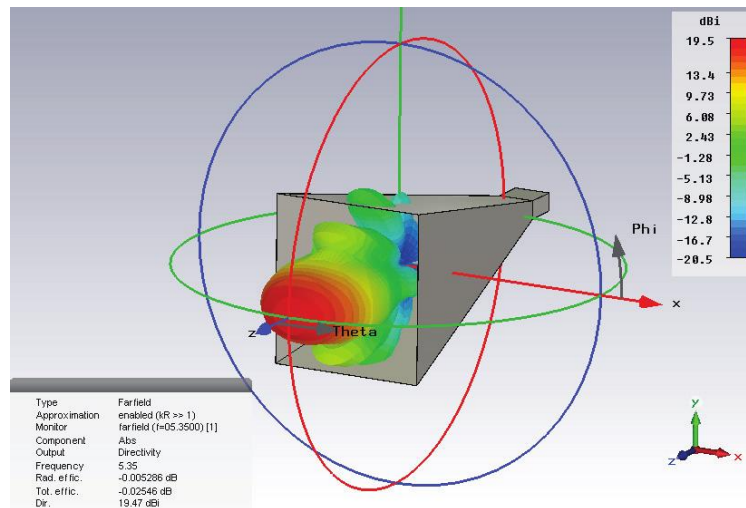


Fig. 15: Aperture Antenna Radiation Pattern

1.1.4 Radio Telescopes:

Optical telescopes collect visible light and concentrate it to a certain point. In the same manner, radio telescopes collect radio waves (also part of the electromagnetic spectrum), concentrate or focus them to a certain point, and allow instruments attached to the telescope (like an amplifier) to process the signals. Radio telescopes are used to study naturally-occurring radiation coming from extra-terrestrial sources such as the Sun, planets in the solar system, stars, clusters, nebulae, interstellar clouds, and so on. The term ‘radio telescope’ usually refers to the entire antenna, feed, receiver, and signal processing setup. Radio telescopes detect portions of the electromagnetic spectrum whose wavelengths range from 0.1cm to 10m. These wavelengths are extremely large compared to visible light, whose wavelengths are on the order of nanometres. For this reason, radio telescopes are the largest telescopes in the world. Otherwise, the radiation simply passes through them.

The most common type of radio telescope is the parabolic dish receiver. Parabolic dish telescopes are a class of antennas called reflector antennas. Reflector antennas have the highest gain out of any antenna type and are extremely directional. This makes them ideal for receiving radiation from point sources. Parabolic radio telescopes generally have a dish attached to a movable mount. There is a feed antenna at the focus of the dish, which actually receives the radiation and sends it for analysis through a waveguide to a detector. The diagram of a radio telescope is shown below:

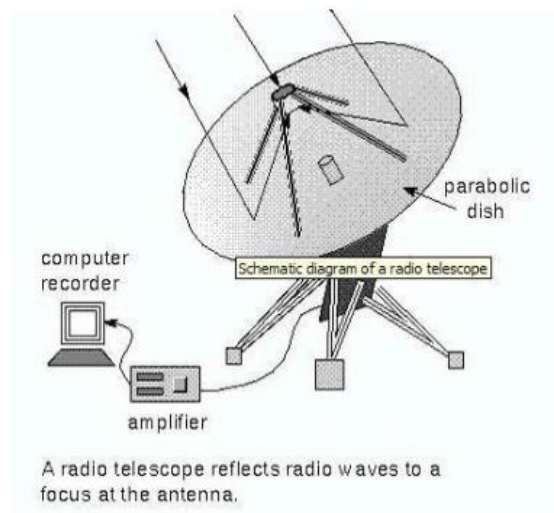


Fig. 16: Radio Telescope

1.1.5 Amateur Radio Astronomy:

With the advent of modern electronics, it has become easier and easier for the amateur to set up a small-scale radio telescope to detect radiation from the galaxy. To detect radiation from the Milky Way, all one needs is some sort of large structural antenna (such as a TV dish) and freely-available spectrometric software, as well as a software-defined radio that acts as a super heterodyne receiver. The total cost of these components comes to just around 7000 rupees for a bare minimum setup. Amateur radio astronomy is popular with hobbyists around the world precisely for these reasons. Although there is very little precision in amateur radio telescopes, the nature of the observations makes results easy to get.

1.2 Literature Review

There are several radio telescopes designs available on the internet. One of the most prominent designs is MIT's Small Radio Telescope (SRT). [6] It consists of a 1.8m parabolic dish attached to a movable altitude-azimuthal (altazimuth) mount with off-the-shelf electronics used in its filtering and amplifying circuit. Intended as a teaching tool, this design was for many years the standard at educational institutions all across the world. Sold as a kit from Cassi Corporation until 2012, this design was surprisingly powerful given its small size. Unfortunately, due to the component shortage caused by COVID-19, it is no longer feasible to create this telescope due to the continuing unavailability of important components. This telescope uses a mixture of Butterworth filters and attenuators as well as a helical antenna to provide the appropriate impedance required for proper detection.

Harvard [7] created a horn antenna for educational outreach. While not as intricate as MIT's, it does use the basic design all horn antennas do. A combination of band pass filters and low noise amplifiers are used in order to receive the signal. The horn antenna is designed for a gain of 13dB. However, this antenna is made out of aluminium foil with cardboard used as a support. Therefore, it does not provide the gain a purely metallic antenna of its size would.

A project called Open Source Radio Telescopes [8] (OSRT) provides designs for a loop antenna used to detect solar flares based on naval signals. However, this method is not efficient in detecting the neutral hydrogen line because of the size of the loop antenna required for such a high frequency.

DSPIRA [9] designs a horn antenna for 17dB of gain, made out of commercially available paint cans. Their horn antenna provides a gain of 16dB in practical use. The SDR spectrometer used is Pluto SDR, in contrast to the more commonly-used spectrometers such as SDR Sharp and Virgo.

Paper [10] constructs a conical horn antenna, in contrast to the rectangular horn antennas generally constructed. Conical horn antennas use cylindrical waveguides and are used to get exactly the same H-plane and E-plane beam characteristics. However, they are difficult to construct and operate, and are susceptible to malfunctioning if the dimensions are altered in any way.

Paper [5] extends a rectangular waveguide with a flare made out of cardboard and provides aluminium foil as the conducting material for the horn antenna. They use a double amplifier-filter setup, with the first signal amplification taking part after the low noise amplification. The signal is then transported with an LMR200 cable to a receiving station, which then uses a hairpin Chebyshev filter in order to filter out even more noise, before the signal is boosted again and is analysed on the computer.

1.3 Motivation

Professional radio telescope installations offer many years' worth of data and are used by professional physicists to perform research. However, it is still possible to probe the universe on a shoestring with small-scale antennas. Important astronomical results, such as the rotational speed of the Milky Way, can be derived with small-scale setups. Most visible-light emissions from the universe are opaque to Earthly observers because of blocking by dust clouds and other gravitational effects. However, due to the large wavelength of neutral hydrogen emissions, the radiation mostly ignores gas particles present in dust clouds. Thus, studying neutral hydrogen emissions opens up a window to the universe that is simply not possible with studying optical emissions. It is also interesting to note that the frequency which neutral hydrogen emits at is almost attenuated by Earth's atmosphere, and no major satellites or communications systems rely on communication at this frequency.

Having a radio observatory, even on a small scale at COEP provides an educational tool for future undergraduates which can then spark an interest in astronomy. Due to the hands-on nature of these observations and the immediate results observed, undergraduates can see the application of engineering methods to radio astronomy. As radio astronomy is immensely multidisciplinary, it allows students from all branches to apply their talents and make the most out of the small radio telescope's observations.

1.4 Aims and Objectives

The purpose of a radio telescope is to observe emissions of neutral hydrogen in the universe. From these emissions, one can divine the type of object emitting them, as well as the object's internal configuration and relative velocity to the Earth. This allows us to derive important astronomical results such as the size and speed of the galaxy, as well as its shape. The methods used all rely on observational data and hence are not susceptible to theoretical misunderstandings.

The design proposed in this report is significantly larger than many other small-scale radio telescopes operating across the world. In conjunction with atmospheric attenuation algorithms and custom spectrometers, our radio telescope can provide significantly more accurate observations and readings compared to other amateur radio telescopes.

1.5 Problem Statement

Roughly 75% of all normal matter in the universe is made up of hydrogen, most of which has not ionized or undergone fusion and fission processes. The emergence of neutral hydrogen atoms throughout the universe occurred during the recombination epoch after the Big Bang, allowing electrons to bind themselves to protons due to the low temperatures of plasma. Due to the abundance of neutral hydrogen in our galaxy, there are many interesting sources of radio emissions.

Emissions from neutral hydrogen sources are suitable for observing because visible light is blocked due to the presence of dust clouds in the interstellar medium (ISM). The Earth's atmosphere is also nearly transparent to this particular type of radiation. Our objective is to design a strong amateur radio telescope which provides gain significantly larger than other designs of the same type, as well as create software that provides comparable results to commercially-available software for analysing results obtained through commercial software-defined radios.

Layout of Project

The aim of this project is to create a radio telescope that can detect interstellar emissions as well as detect the Sun, whose proximity to the Earth allows detection at many frequencies. Our simulation of the required horn antenna is done in Ansys HFSS. We then construct this horn antenna and take readings of the Milky Way and the Sun. Simulation model is developed in Simulink whereas the algorithm is developed in MATLAB.

The objective that we want to achieve in this project is to develop a high-gain radio telescope for educational purposes. This will help in bringing astronomy to the masses. Chapter 1 elaborates on the problem statement of the project along with introduction to some basic terms. Several fault location algorithms as discussed in literature review are jotted down in Chapter 3. The proposed method is elaborated in Chapter 4. Effect of charging current is neglected in each method. Several existing algorithms are tested using real time data in the Chapter 5. The results those were obtained are tabulated. Chapter 6 consist of conclusion, future scope, references and acknowledgement.

Chapter 2

2.1 Horn Antenna Design

We chose to design a horn antenna for our radio telescopes. As mentioned previously, horn antennas are an example of antenna types known as aperture antennas. In aperture antennas, radiation occurs from an aperture. To provide an effective gain, aperture-type antennas must have an aperture length and width of at least several wavelengths. This is the reason why aperture antennas are used the most in the microwave portion of the electromagnetic spectrum, where the frequencies are in the order of centimetres. Horn antennas also do not have resonant elements; they can therefore operate over a large range of frequencies. The beam width of horn antennas is also relatively high and the performance of the horn antenna remains stable over a large range of frequencies. Horn antennas have good gain and good directivity. They avoid the phenomenon of standing waves, but provide lesser reflection.

Horn antennas are generally used as feeds for parabolic dishes. This is because the antenna itself has an ellipsoidal radiation pattern and is not suited for making very precise observations. This can be mitigated by using a parabolic dish, whose radiation pattern is extremely directional. However, the horn antenna on its own provides a large amount of gain. Due to the nature of parabolic antennas, the receiver must be placed at the focus. This means that the receiving horn will need extremely large dishes for it to function properly. The size of the dish increases exponentially with the size of the horn antenna.

We have chosen to construct a pyramidal horn antenna. The two main types of horn antennas are H-plane and E-plane horn antennas.

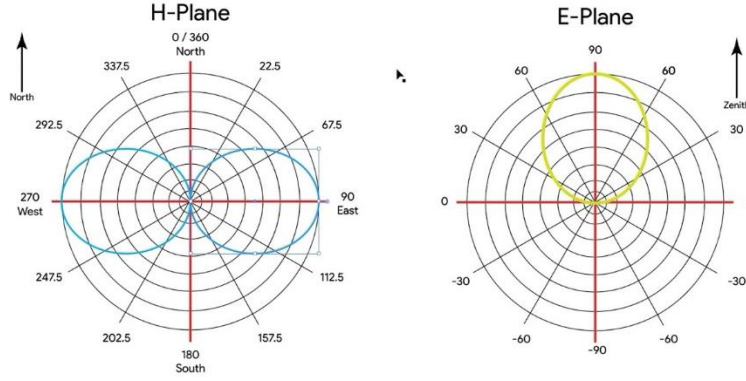


Fig. 17: H plane and E plane Horn Antenna

E-plane and H-plane are two terms used mostly in microwave antenna designs. The E-plane is the plane containing the electric field vector and the direction of maximum radiation. Similarly, the H-plane is the plane containing the magnetic field vector and the electric field vector. The E-plane and the H-plane are at $\frac{\pi}{2}$ radians to each other.

Consider a rectangular aperture of dimensions $2a$ by $2b$ in the XY plane with the Z-axis pointing outwards.

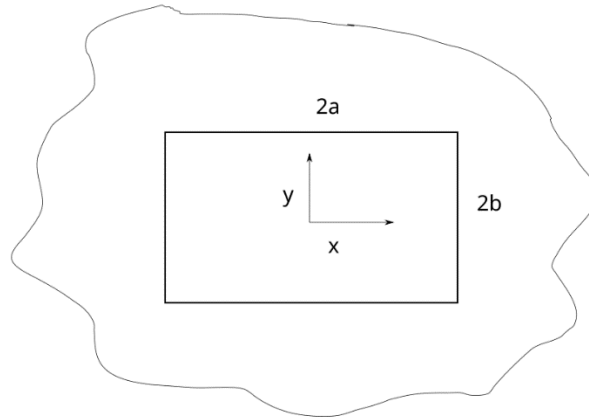


Fig. 18: Uniform Electric Field across the aperture

Assume that there is a uniform electric field across the aperture. This assumption is strictly not required but it can be made for ease of calculation. The electric field can then be given by $E_x = E_0 \hat{i}$. The Fourier transform of the aperture field is then given by:

$$f_t = E_0 \hat{i} \int_{-a}^a \int_{-b}^b e^{jk_x x + jk_y y} dy dx$$

Solving this integral, we obtain $f_t = 4abE_0 \hat{i} \frac{\sin u}{u} \frac{\sin v}{v}$ where $u = k_0 a \sin \theta \cos \phi$ and $v = k_0 b \sin \theta \sin \phi$. The radiated electric field is given by

$$E(r) = jk_0 \frac{e^{-jk_0 r}}{2\pi r} [a_\theta (f_x \cos \phi + f_y \sin \phi) + a_\phi \cos \theta (f_y \cos \phi - f_x \sin \phi)]$$

Therefore, the radiated electric field by the rectangular aperture is simply

$$E(r) = \frac{jk_0 4abE_0}{2\pi r} e^{-jk_0 r} \frac{\sin u}{u} \frac{\sin v}{v} (a_\theta \cos \phi - a_\phi \sin \phi \cos \theta)$$

This expression tells us that the radiation pattern has an extremely large central lobe with side lobes falling off drastically. This makes the horn antenna a good transmitter. Using the principle of reversibility, the horn antenna is an extremely good receiver when radiation is fed into it in a heavily directional manner.

Consider an H-plane sectoral horn

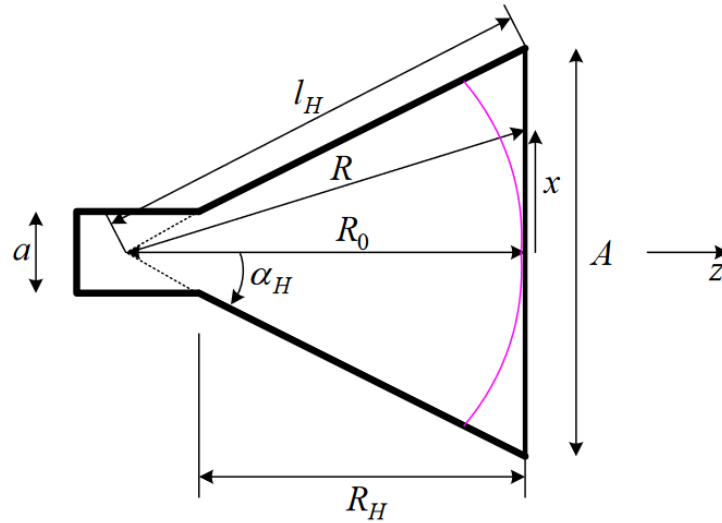


Fig. 19: H-plane sectoral horn

It is instantly seen that $l_H^2 = R_0^2 + \left(\frac{A}{2}\right)^2$ and $\alpha_H = \arctan \frac{A}{2R_0}$. Also

$R_H = (A - a)\sqrt{\frac{l_H}{A} - \frac{1}{4}}$. The field that arrives at the input of the horn is composed of the transverse field components of the dominant mode of propagation in the waveguide, TE_{10} . Therefore, $E_y(x) = E_0 \cos(\frac{\pi}{a}x)e^{-j\beta_g z}$ and $H_x(x) = \frac{-E_y(x)}{Z_g}$.

$Z_g = \frac{\eta}{\sqrt{1 - (\frac{\lambda_0}{2a})^2}}$ is the wave impedance of the TE_{10} waveguide mode and $\beta_g = \beta_0 \sqrt{1 - (\frac{\lambda_0}{2a})^2}$ is the propagation constant of that mode. Here $\beta_0 = \frac{2\pi}{\lambda_0}$ where λ_0 is the free-space wavelength. It should be noted that as A increases, the wave impedance of the open horn approaches the impedance of free space. This is part of the reason why it is required to find a balance between the aperture flare and the required gain.

The waves arriving at the horn aperture are not in phase. They take different paths inside the horn while traveling from the horn apex to the horn aperture. This phase variation is given by $e^{-j\beta(R-R_0)}$. Since our aperture is not flared along the y-direction, the path of the wave in the horn can be approximated by $R = R_0[1 + 0.5(\frac{x}{R_0})^2]$.

Now, if $x \ll R_0$, then this can be further approximated as $R - R_0 = 0.5 \frac{x^2}{R_0}$.

Therefore, the field at the aperture is $E_{a_y}(x) = E_0 \cos(\frac{\pi x}{A})e^{-j\frac{\beta}{2R_0}x^2}$

A similar result can be derived for the H-plane sectoral horn, pictured below:

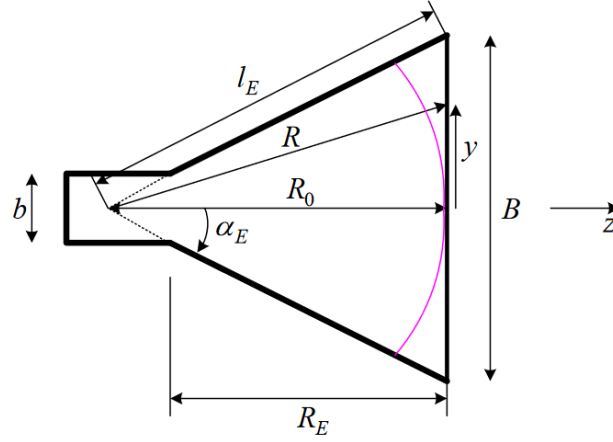


Fig. 20: E-plane sectoral horn

$$E_{a_y} = E_0 \cos\left(\frac{y}{a}\right) e^{-j \frac{\beta}{2R_0} y^2}$$

The pyramidal horn antenna is a combination of both the H-plane and E-plane sectoral horn antennas.

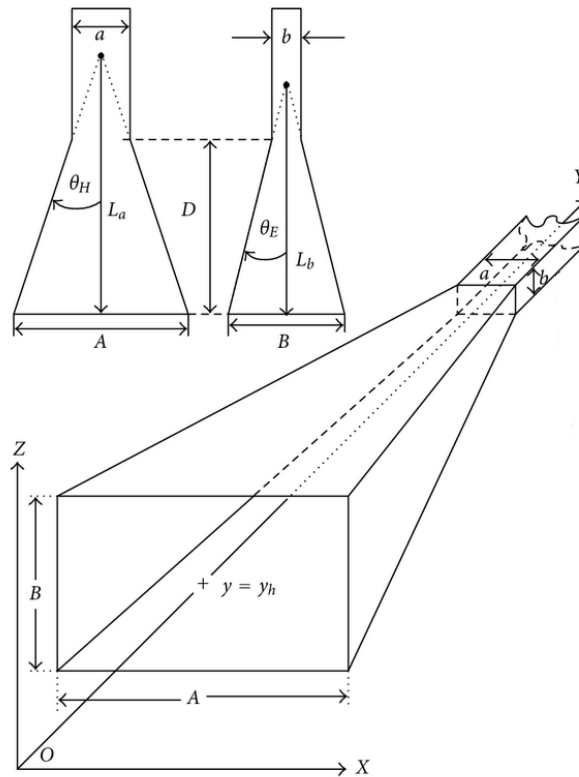


Fig. 21: Pyramidal Horn Antenna

The principle of superposition can therefore be applied and the field distribution at the aperture is therefore:

$$E_{a_y} = E_0 \cos\left(\frac{\pi x}{A}\right) e^{-j\frac{\beta}{2}\left(\frac{x^2}{R_0^E} + \frac{y^2}{R_0^H}\right)}$$

The maximum theoretical efficiency of a horn antenna is approximately 0.51.

2.2 Optimum Pyramidal Horn Design

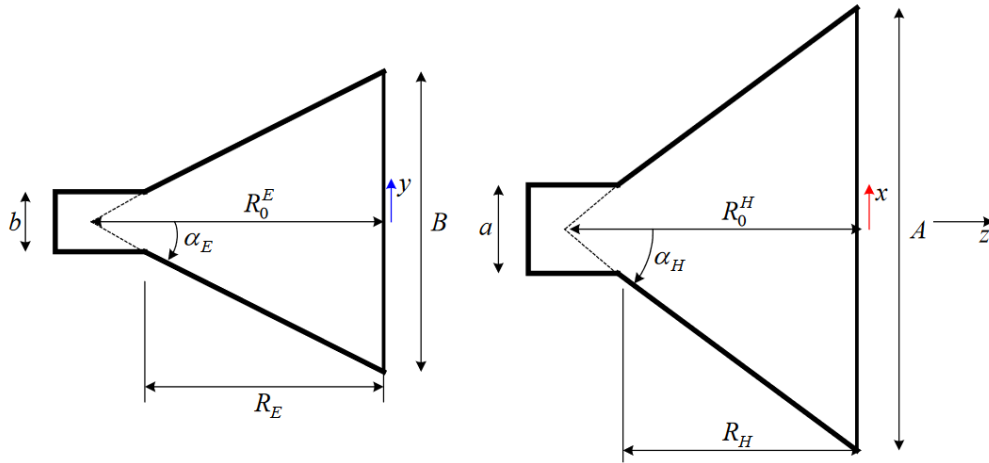


Fig. 22: Optimum Pyramidal Horn Antenna

The values of R_0^E and R_0^H are in proportion with R_E and R_H respectively by the Basic Proportionality Theorem. The gain of the horn antenna is given by $G = \frac{4\pi}{\lambda^2} \epsilon_{ap} AB$. The optimum relation between the flare height B and the horn apex length R_0 that produces the maximum possible directivity is $B = \sqrt{2\lambda R_0}$. Substituting this in the results obtained by the Basic Proportionality Theorem, the relation between B and R_E is obtained:

$$B = \frac{1}{2}(b + b\sqrt{b^2 + 8\lambda R_E}).$$

Similarly, $A = \sqrt{3\lambda R_0}$. Therefore, the relation between A and R_H is obtained:

$$A = \frac{A - a}{3\lambda R_H}.$$

For the horn to be physically realized, $R_H = R_E$. Therefore, a relation between B and A is obtained:

$$B = \frac{1}{2}(b + \sqrt{b^2 + \frac{8A(A - a)}{3}}).$$

Combine this with the gain equation to get the **Ideal Horn Equation**:

$$A^4 - aA^3 + \frac{3bG\lambda^2}{8\pi\epsilon_{ap}}A - \frac{3G^2\lambda^4}{32\pi^2\epsilon_{ap}^2} = 0.$$

It should be noted that the unknown variable A does not particularly matter. The same equation can be written in B as well.

This equation is for an ideal horn, which we modify to include wave reflections.

2.3 Modified Horn Antenna Design

The on-axis gain of pyramidal horns is influenced by a number of factors. When calculating gain, it's common to assume that only the dominant mode TE_{10} is present and propagating within the antenna; however, this isn't the case since as the antenna's dimensions grow larger, other higher-modes will develop in the antenna aperture, modifying the antenna's gain. In addition, because wave reflections propagate inside the antenna, they are not included in the formulae. Waves undergo reflection as the size of the aperture increases, raising the VSWR value. There will be fewer reflections and better impedance matching if the transition from waveguide to free space is smooth,

resulting in higher operational bandwidth. [New Method for Optimum Design of Pyramidal Horn Antennas, Journal of Microwaves, Optoelectronics and Electromagnetic Applications, Vol. 10, No. 1, June 2011]

This happens when the antenna's flare or aperture angle is small and the length of the antenna is large. The oscillation of pyramidal gain that is seen in the plot of gain versus frequency due to numerous diffractions on the aperture margins of the E-plane with further refractions on the antenna wall is another element that is not generally taken into account. With increasing frequency, these oscillations become smaller and smaller; however, they are important at lower frequencies.

Define $R_0^H = R_1$ and $R_0^E = R_2$. The phase error in the H-plane (assumed constant)

is usually defined by $t = \frac{A^2}{8\lambda R_1}$ and the phase error in the E-plane is usually defined

by $s = \frac{B^2}{8\lambda R_2}$. We introduce a modified version of t and s , denoted by t_e and s_e respectively, following the method proposed by Pereira et al. Therefore, the following formulas come about:

$$t_e = \left(\frac{A}{\lambda}\right)^2 \frac{1}{8t} \left(\sqrt{1 + \left(\frac{\lambda}{A}\right)^2 16t^2} - 1 \right)$$

$$s_e = \left(\frac{B}{\lambda}\right)^2 \frac{1}{8s} \left(\sqrt{1 + \left(\frac{\lambda}{B}\right)^2 16s^2} - 1 \right)$$

Therefore, it is easily seen that $A = 2\sqrt{t_e\lambda(t_e\lambda + 2R_1)}$ and $B = 2\sqrt{s_e\lambda(s_e\lambda + 2R_2)}$. Therefore, from the formula of gain, we can isolate R_1 and R_2 in order to obtain the **Modified Horn Equation**:

$$0 \quad \frac{B^4}{8\lambda_3} - \frac{1}{\lambda} \left(\frac{b}{s_e} + \frac{2\pi a \epsilon_{ap} t_e}{G} \right) B^3 + \frac{\lambda}{2} (t_e - s_e) B^2 + \lambda \left(\frac{s_e b}{2} + \frac{aG}{32\pi \epsilon_{ap} t_e} \right) B - \frac{G^2 \lambda^3}{128\pi^2 \epsilon_{ap}^2 t_e} =$$

The process for designing any antenna is as follows:

1. First decide what frequency you want it to operate at.
2. Decide how much gain you want.
3. Decide other parameters like bandwidth, beam width, return loss, VSWR, etc.
4. Calculate the dimensions based on formulae and run simulations to determine the gain.

Solving this equation by Powell's method, we can obtain the value of B and obtain the value of A based on it. These are all the values needed to design a horn antenna.

It should be noted that the only values left are a and b , the waveguide aperture values. These values are not so easy to precisely calculate, and thus must be arrived at experimentally, which is explained in the next section.

2.4 Waveguide Design

Waveguides are physical structures that guide waves. In the context of antenna theory, they are structures made out of conducting material that offer a way for electromagnetic waves to propagate to a desired location with minimal loss of energy. If there is no waveguide, then the intensity of a wave propagating through free space decreases according to the inverse-square law.

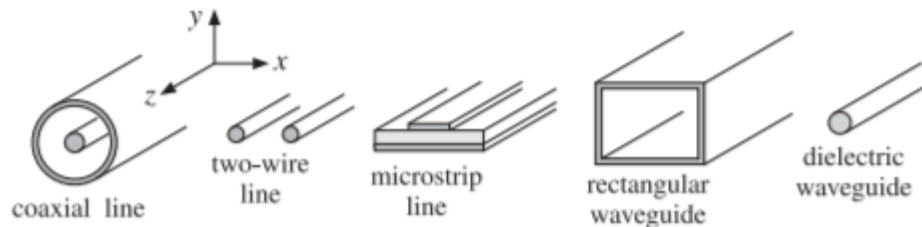


Fig. 23: Types of waveguide

Waveguides are the part of horn antennas that primarily determine the frequency that the horn antenna operates at. Waveguides can act as band-pass filters, particularly rectangular waveguides. They do not allow waves above and below certain frequencies to pass through without heavy attenuation.

In any waveguide system, we look for a solution of Maxwell's equations such that the direction of propagation is along the z axis and the boundary is defined at the physical boundary of the waveguide. The electric and magnetic fields therefore have the form:

$$E(x, y, z, t) = E(x, y)e^{j\omega t - j\beta z}$$

$$H(x, y, z, t) = H(x, y)e^{j\omega t - j\beta z}$$

Here $\beta = \frac{2\pi}{\lambda_g}$, where λ_g is the **Guide Wavelength**.

Since the propagation is along one particular direction, the fields are not uniform and hence their dependence on x and y cannot be trivial.

The method to approach this involves decomposing the fields into transverse and longitudinal forms:

$$E(x, y) = E_t(x, y) + \hat{z}E_z(x, y)$$

$$H(x, y) = H_t(x, y) + \hat{z}H_z(x, y)$$

Since the energy transfer, and hence the power transfer must necessarily take place along the z direction, the transferred power can be written in terms of the integral of the Poynting vector as follows:

$$P_t = \int_S P_z dS$$

where $P_z = \frac{1}{2} \text{Re}(E_t \times H_t) \cdot \hat{z}$

Losses occur inside a waveguide due to the natural resistance of the conducting material as well as the effect of the material filling the space in between the conductors. This type of loss is called the dielectric loss and must be accounted for. To account for this, we replace, β the propagation wavenumber, by a complex-valued number $\beta - j\alpha$, where α is called the attenuation constant. Therefore, the z-component of all fields is replaced as follows:

$$e^{-j\beta z} \rightarrow e^{-\alpha z} e^{-j\beta z}.$$

Note that α is the sum of all attenuation constants, which may include the Ohmic losses, dielectric losses, etc.

The skin depth of the conductor is a measure of how deep electric currents are formed in the conductor when an electromagnetic field interacts with it. This is approximated

by $\delta = \sqrt{\frac{2}{\omega\mu\sigma}}$, where the symbols have their usual meanings. It should be noted that the skin depth depends on the magnetic propagation characteristics of the medium. Substitution with actual values of a good conductor, say, aluminium, results in the skin depth being of the order of a few micrometres, signifying that the actual amount of material required is very little for aluminium to act as an antenna.

A pyramidal horn antenna requires a rectangular waveguide.

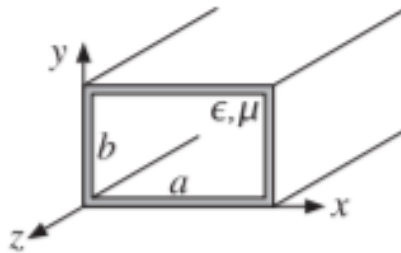


Fig. 24: Rectangular Waveguide

We make two significant assumptions while deriving the equations for the waveguide. The first assumption is that $a > b$. This can be taken without loss of generality. The second assumption is that the rectangular waveguide allows mostly magnetic fields to

propagate through it. This mode of propagation is called the TE mode of propagation and is mathematically equivalent to saying $E_z = 0$ and $H_z \neq 0$. After making this assumption, we can write down the Helmholtz equation:

$$\partial_x^2 H_z(x) + k_c^2 H_z(x) = 0$$

The general solution of this equation is a linear combination of sines and cosines of $k_c x$. However, our boundary conditions stipulate that $H_z = 0$ at $x = 0$ and $x = a$. Therefore, the solution is necessarily of the form $H_z(x) = H_0 \cos k_c x$ where H_0 is a complex-valued constant. Since there is no dependence on y , we can safely put $H_y = 0$ and $E_x = 0$.

We define $H_1 = \frac{j\beta}{k_c} H_0$ and $E_0 = -j\eta \frac{w}{w_c} H_0$.

It follows that $H_x(x) = H_1 \sin k_c x$ and the corresponding electric field is $E_y(x) = E_0 \sin k_c x$.

Now we have obtained the three non-zero components of the electromagnetic field. Our boundary conditions are derived using a perfectly conductive wall, which means that there is no tangential electric field at any of the wall sides. Therefore, $E_y(x)$ vanishes on the left side of the conductive wall and on the right side ($x = a$) the solution implies that $\sin k_c a = 0$. This means that $k_c = \frac{n\pi}{a}$ and therefore we obtain the TE_{n0} modes of propagation.

Similarly, it is possible to derive TE_{nm} modes of propagation. However, we have derived that the propagation of the electric field through the waveguide is negligible. Therefore, the only mode of propagation present is TE_{n0} propagation, and the cut-off frequencies for different modes are given by:

$$\lambda_{n0} = \frac{1}{\sqrt{\left(\frac{n}{2a}\right)^2}}$$

Since the dominant mode of propagation depends only on the length of the waveguide, it is natural to question what the height of the waveguide must be while physically making one. All waveguides systems operate in a frequency range that ensures only the lowest mode can propagate. This is because of the errant noise and uncertainty over which mode is actually carrying the necessary signal that will occur if multiple modes are allowed to propagate. A wave will only propagate if its frequency is greater than the cutoff frequency. Waves with frequencies lower than the cutoff frequencies will attenuate exponentially along the waveguide as they propagate.

To arrive at the value of b , it is necessary to ask what happens to the transmitted power if the waveguide is allowed to operate in its dominant mode of propagation. We know the transferred power is calculated by integrating the Poynting vector; therefore, it is easy enough to integrate the Poynting vector for the non-zero field components.

$$P_z = \frac{1}{2\eta_{TE}} |E_t|^2$$

Integrating over the cross-sectional area of the guide, we obtain:

$$P_t = \int_0^a \int_0^b P_z dx dy$$

which results in
$$P_t = \frac{1}{4\eta_{TE}} |E_0|^2 ab$$

The power transmitted is proportional to the product ab . Therefore, to have the maximum power possible, it is necessarily to choose b such that it also satisfies the maximum bandwidth. Therefore, we pick $b = \frac{a}{2}$ in order to get the maximum power and bandwidth.

Now that we have b , the final question is to calculate a . This is not as easy as it appears. Other projects use commercial waveguides designed to operate in a set frequency region. Oftentimes, the waveguide used is a WR650 waveguide, named for its dimensions (6.5 inches x 3.25 inches). The recommended frequency range is 1.15 to 1.72 GHz (<https://www.everythingrf.com/tech-resources/waveguides-sizes>) and the

lowest cutoff frequency is 0.908 GHz. In general, rectangular waveguides are supposed to operate at 1.25-1.89 times the lowest cutoff frequency. Keeping this in mind, we simply take the required center frequency as the average - $f_{req} = 1.57f_{c,lowest}$ and calculate the RHS based on our requirement - in this case, the hydrogen line.

This results in our cut off frequency being $0.904 \times 10^9 GHz$, and hence the dimension for a being $16.56cm$. The value of b , is therefore $8.28cm$. For our horn antenna, we arbitrarily select the gain to be 20dB. Note that in power laws, the decibel is defined as $10\log_{10}quantity$ compared to RMS laws. Now that we have the values of a , b , G , and λ , we can calculate B by the modified horn equation, and thus we can calculate A using the relationship between A and B derived above.

We wrote a program in Python3.10 to calculate the dimensions of the horn required horn antenna and other dimensions needed for fabrication. The output of the program for 20dB is given below:

```
a in mm: 165.682995325
a in inches: 6.522952571850393
b in mm: 82.8414976625
b in inches: 3.2614762859251964
te 0.402981
Se 0.265178
a 2.2333886053073004
b 0.19495537504392849
c 0.014542427350002721
d 0.17495441647212562
e 0.7387379068787291

fjac: array([[ -1.]])
fun: array([0.] )
```

message: 'The solution converged.'

nfev: 22

qtf: array([2.37476705e-13])

r: array([-3.53814776])

status: 1

success: True

x: array([0.7430115])

A in mm: 954.2035925001858

A in inches: 37.567070570873454

B in mm: 743.0115017758903

B in inches: 29.252421329759464

R1 in mm: 1295.606283519741

R1 in inches: 51.00812139841501

R2 in mm: 1204.9937366871484

R2 in inches: 47.44069829476962

Le in mm: 1260.9625007898023

Le in inches: 49.64419294448041

Lh in mm: 1380.6599023224007

Lh in inches: 54.35668906781105

mechanical_depth in mm: 1070.6438839829775

mechanical_depth in inches: 42.15133401507786

mass 0.33770129623986805

theta_H 36.37134672593528

theta_E 31.658409595735016

$R2/\cos(\theta_H) = 1.4965325518622776$

$R1/\cos(\theta_E) = 1.522107582159228$

Ldash_H in mm: 1140.9292306504087

Ldash_H in inches: 44.91847364765388

Ldash_E in mm: 1120.372453647859

Ldash_E in inches: 44.109151718419646

AreaH 1.2777113430631004

AreaE 0.9252629513332333

6.899641252540742 4.996419937199461

4377.446991025792

r 900.0

109.06313785749607

106.41606874413814

1.1877186611042625

1.1877186611042625

2.5 Coaxial Transition Design

To actually send signals to your radio apparatus, the electromagnetic field must be converted into voltage readings that allow for instruments to pick it up. This forms the coaxial feed for the rectangular waveguide. While there are no precise methods of analysis to design a perfect antenna-transmission line feed, empirical methods allow us to calculate the attenuation due to this transition.

It should be noted that we have derived the dimensions of the horn antenna, but the crucial part left is the depth of the waveguide. None of the formulae so far have involved this depth. It is generally required to calculate a dimension called the **Guide Wavelength**, given by:

$$\lambda_g = \frac{\lambda}{\sqrt{1 - (\frac{f_c}{f})^2}}$$

where f_c is the cutoff frequency for that mode of transmission, f and λ are the inherent wavelength and frequencies of your expected radiation. The guide wavelength for our requirements turns out to be $27.376cm$. The probe is simply inserted in the waveguide

at a distance of $\frac{\lambda_g}{4}$ from the end of the waveguide. To allow for at least one full wavelength to propagate in the waveguide, we choose $1ft = 30.48cm$ as the depth of our waveguide.

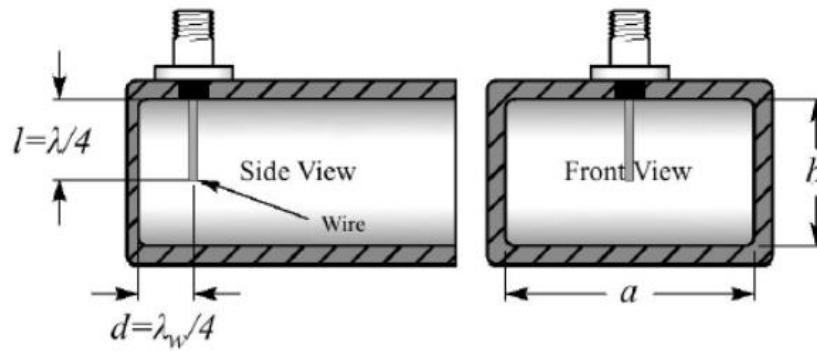


Fig. 25: Waveguide Dimensions

The transition is part of the transmission line, not the antenna, and has no bearing on the antenna's performance. The transition could be immediately at the antenna, appearing to be a part of it, or many meters away at the other end of a waveguide transmission line run. However, because solid-state components are typically built on microstrip transmission lines and interconnected with coax, whereas microwave antennas are typically built using waveguide techniques, the transition is an important feature of most microwave systems.

Chapter 3

3.1 Simulation, Results and Comparison with other commercially viable Available Calculators

Ansys HFSS is the primary tool used for microwave antenna simulations. We simulate the horn antenna in HFSS. A far-field setup is inserted. This is particularly appropriate for radio telescopes because of the distance it receives radiation from. Aluminum was used as the conductive material for the simulation. The method of finite element analysis with adaptive meshing and mixed integrals is used for the simulation. The simulation sweeps from 0.71 GHz to 2.13GHz, taking 401 points in between.

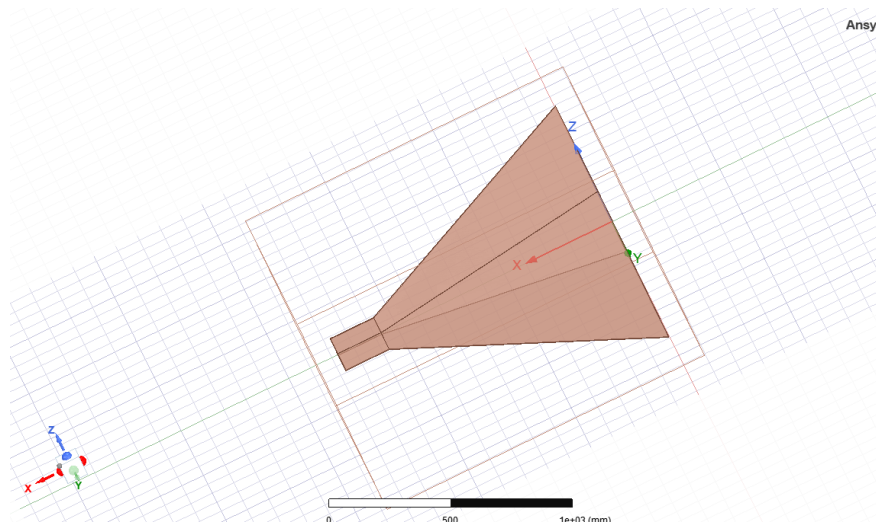


Fig. 26: Horn Antenna Design in Ansys

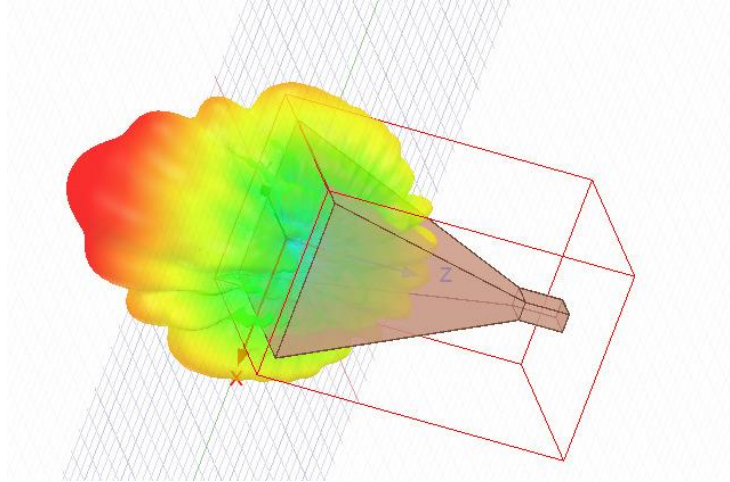


Fig. 27: Horn Antenna Simulation in Ansys

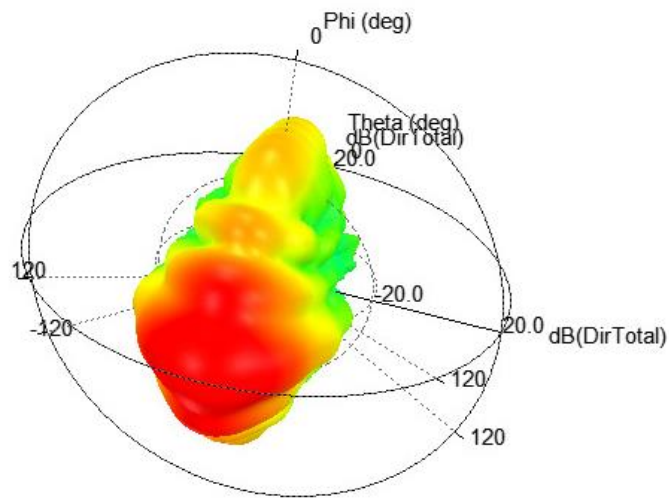


Fig. 28: Horn Antenna Radiation Pattern observed in Ansys

The images above show the directivity of the horn antenna, which reaches a simulated maximum of **19.997 dB** at our designed frequency. Thus, we can conclude that our horn antenna design is similar to theoretical values.

In two-port networks, various parameters called the S-parameters describe the input-output relationship between ports in a system.

For example, S_{12} describes the power transferred from port 1 to port 2. Therefore, S_{11} is a measure of the reflected power of an antenna at a single input port. This particular parameter is the most important parameter describing the capability of an antenna to transfer power. S_{11} is different at different frequencies. It is also called the reflection coefficient or the return loss. The maximum value of S_{11} is 0, as it represents that all of the power is being reflected from the system. Usually measured in dB, the value of S_{11} must be as low as possible at the desired frequency. The simulated S_{11} is shown below, while the real value must be measured with a vector network analyser.

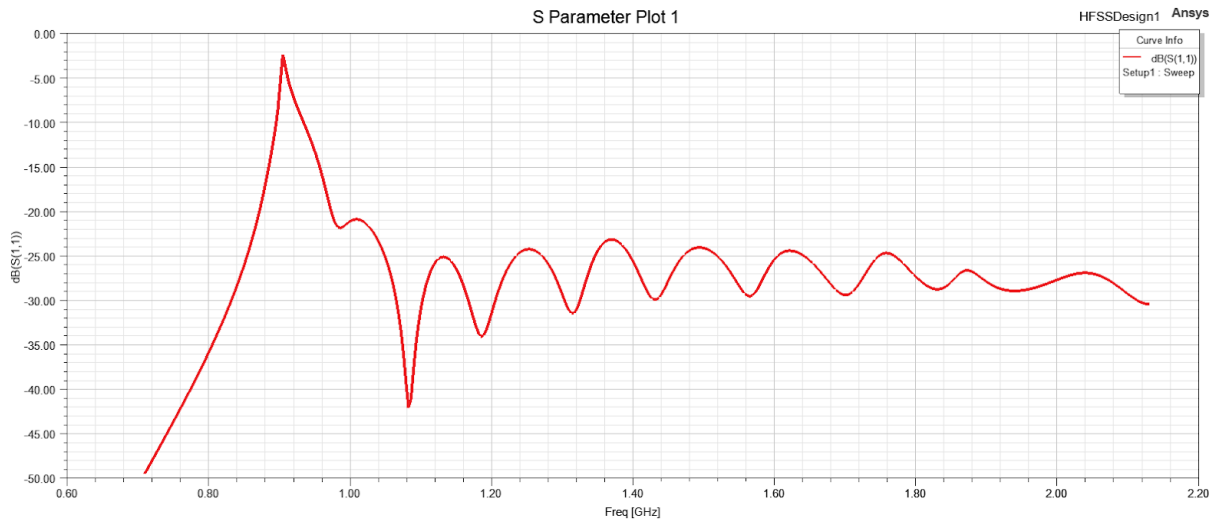


Fig. 29: Simulated S11 pattern

Antennas can be considered as part of transmission lines due to them acting as passive transducers. For this reason, they follow the maximum power transfer theorem, which requires impedance matching at the source and the load. The voltage standing wave ratio (VSWR) is a quantity that is a function of the reflection coefficient. The function is highly non-linear and can be approximated as:

$$VSWR = \frac{1 + |S_{11}|}{1 - |S_{11}|}$$

Unlike S_{11} , it is difficult to tell what a good value of the VSWR should be. VSWR is the ratio of the peak amplitude of a standing wave to the minimum amplitude of a standing wave. A table of VSWR is shown below:

VSWR	(s11)	Reflected Power (%)	Reflected Power (dB)
1.0	0.000	0.00	-Infinity
1.5	0.200	4.0	-14.0
2.0	0.333	11.1	-9.55
2.5	0.429	18.4	-7.36
3.0	0.500	25.0	-6.00
3.5	0.556	30.9	-5.10
4.0	0.600	36.0	-4.44
5.0	0.667	44.0	-3.52
6.0	0.714	51.0	-2.92
7.0	0.750	56.3	-2.50
8.0	0.778	60.5	-2.18
9.0	0.800	64.0	-1.94
10.0	0.818	66.9	-1.74
15.0	0.875	76.6	-1.16
20.0	0.905	81.9	-0.87
50.0	0.961	92.3	-0.35

Table 1: VSWR

In general, the value of VSWR should be under 2, as changes in the VSWR at higher values don't affect the performance of the antenna that much. The VSWR for our horn antenna through simulations is shown below:

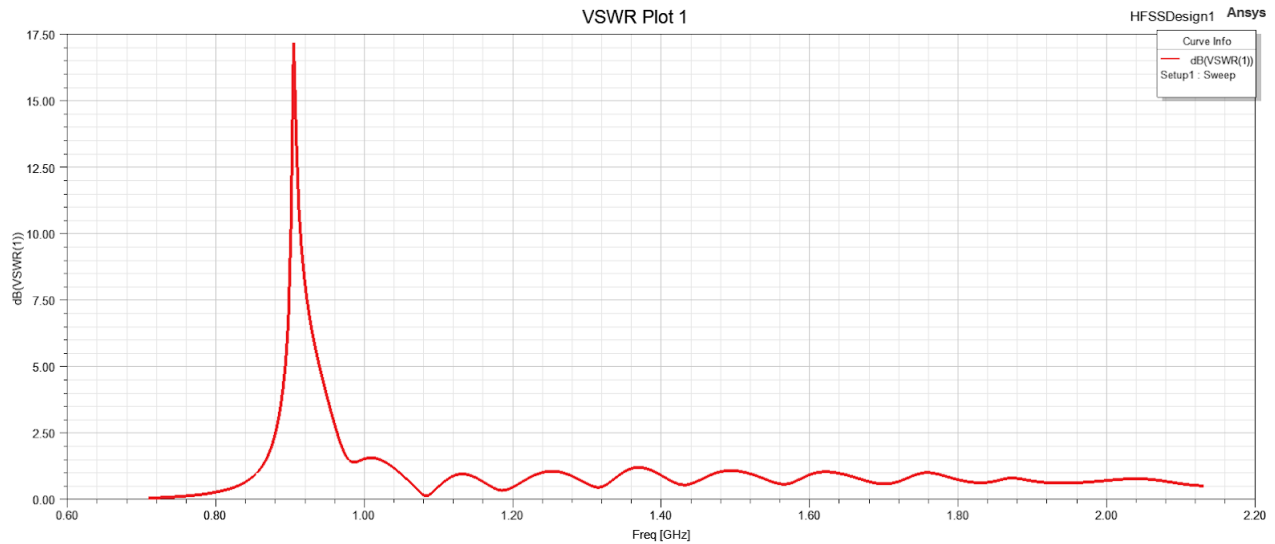


Fig. 30: VSWR through simulations

Observe the high peak approximately $0.9GHz$. This indicates that the waveguide does indeed act as a band pass filter, as evidenced by the high VSWR at the lowest cut-off frequency.

The Smith chart for the S-parameter is as follows:

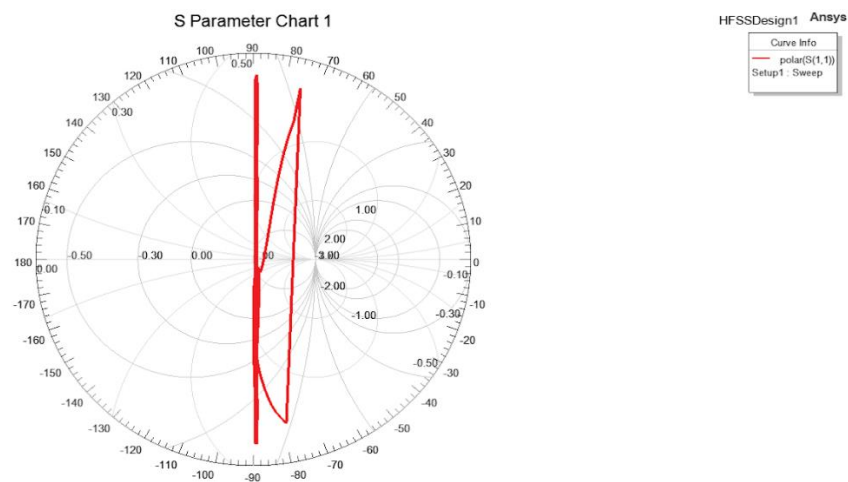


Fig. 31: Smith chart for S parameter

It is clearly seen $0.9GHz$ that the waveguide of the horn antenna acts as a band pass filter for frequencies below and above $1.8GHz$.

The performance of the pin feed is as follows:

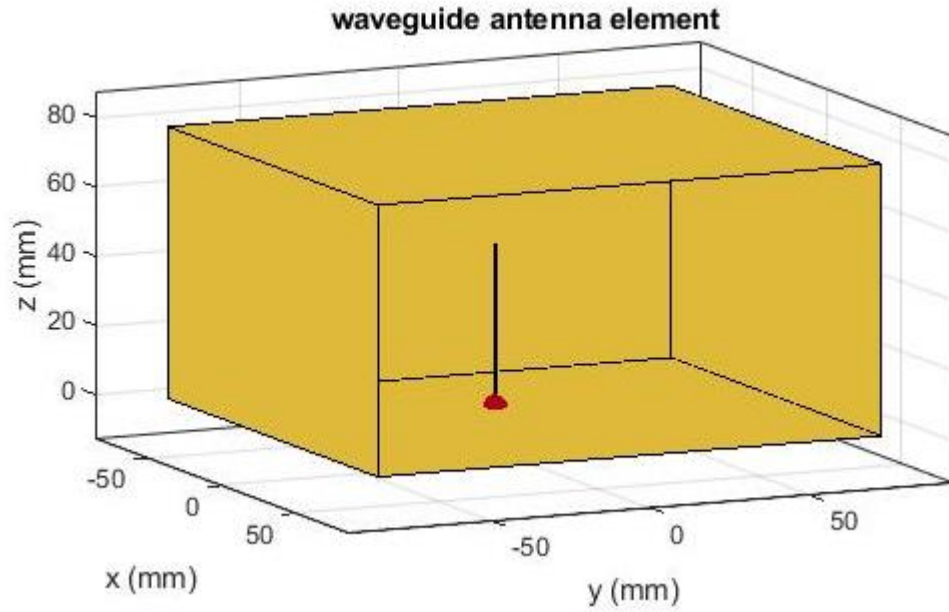


Fig. 32: Waveguide Antenna Element

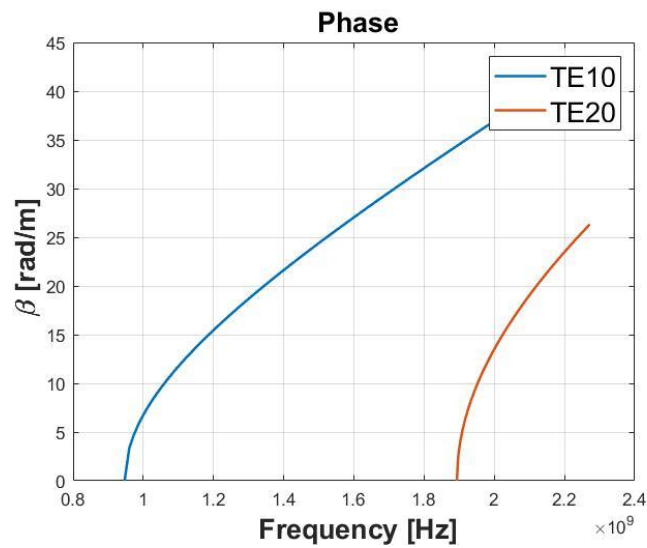


Fig. 33: Performance of Pin Feed- Phase

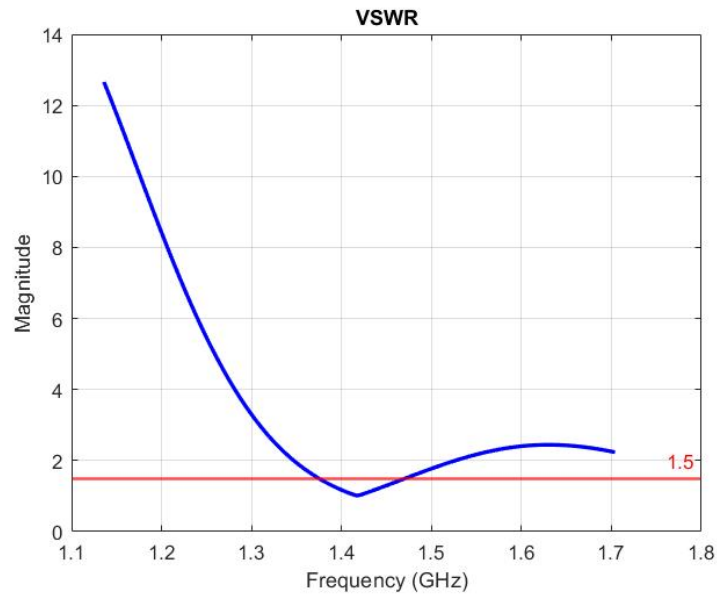


Fig. 34: Performance of Pin Feed- VSWR

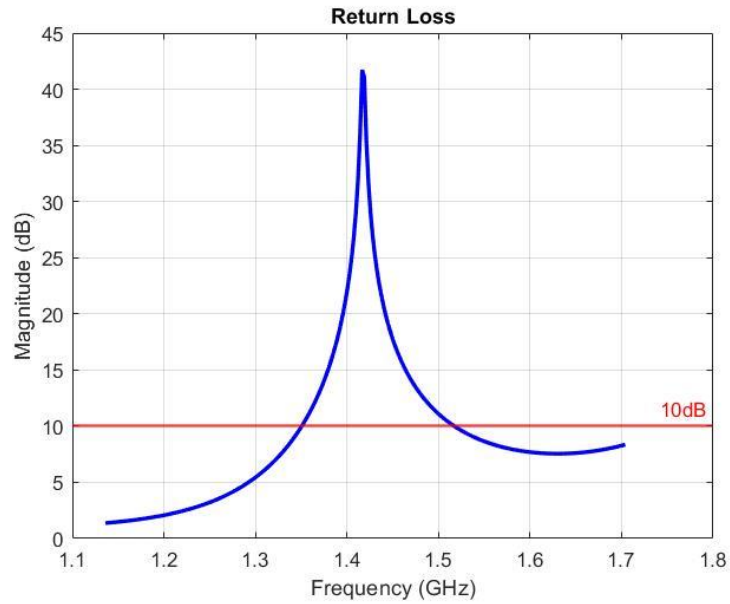


Fig. 35: Performance of Pin Feed- Return Loss

So far, we have simulated the horn antenna using finite-element methods of analysis. Other solvers exist, some of which simulated RF-network performance. This method of analysis dates back to times before numerical solvers were available. The implementation of our requirements in one of these solvers results in a horn antenna that is less than half the size of our design in HFSS. However, the simulation shows

that the maximum possible gain a pyramidal horn antenna this size can achieve is just above 10dB, which is not suitable for our requirements. This simulation was run using MATLAB, and the results are shown below.

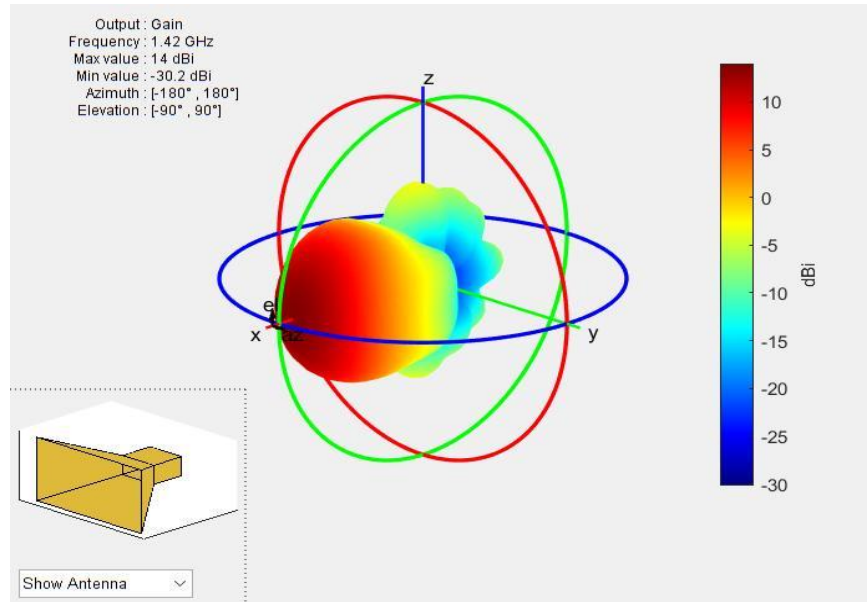


Fig. 36: Simulation Result

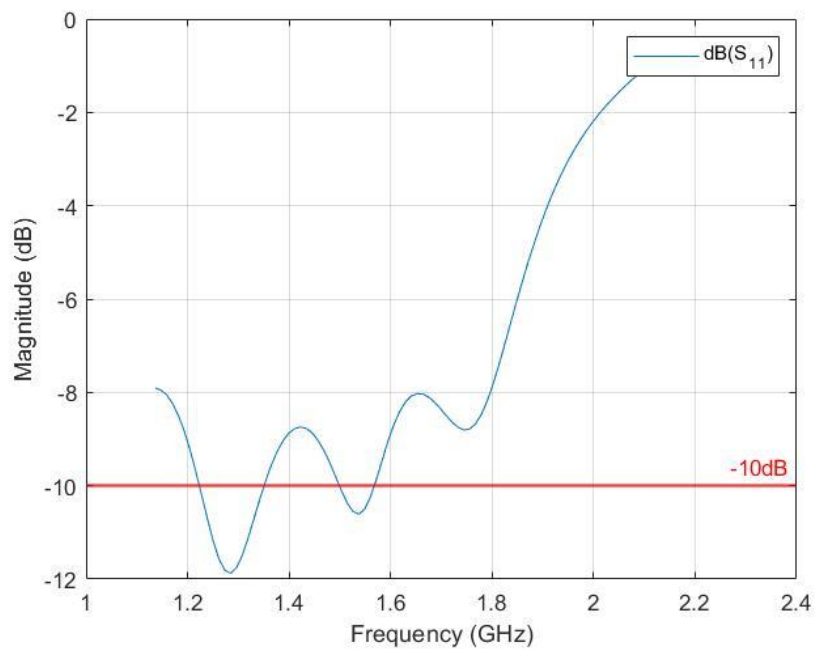


Fig. 37: Simulation Result

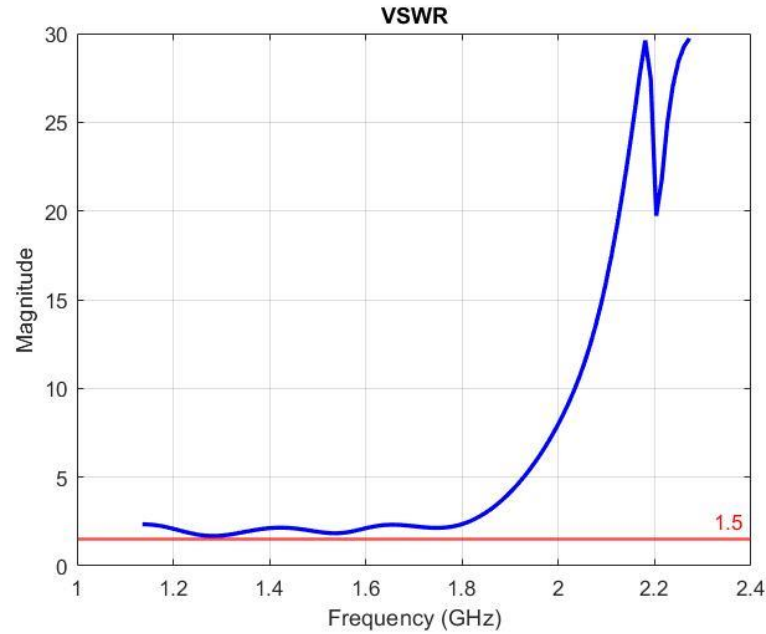


Fig. 38: Simulation Result

In fact, we observe that the VSWR and the return loss parameters drastically differ from the simulation performed using HFSS.

3.2 Atmospheric Attenuation

The International Telecommunications Union (ITU) provides formulae for empirically approximating the atmospheric attenuation at certain frequencies over a certain time period. We used ITU-RPy, the Python implementation of these formulae, to estimate the transparency of the atmosphere to 1.42GHz. The results are plotted below:

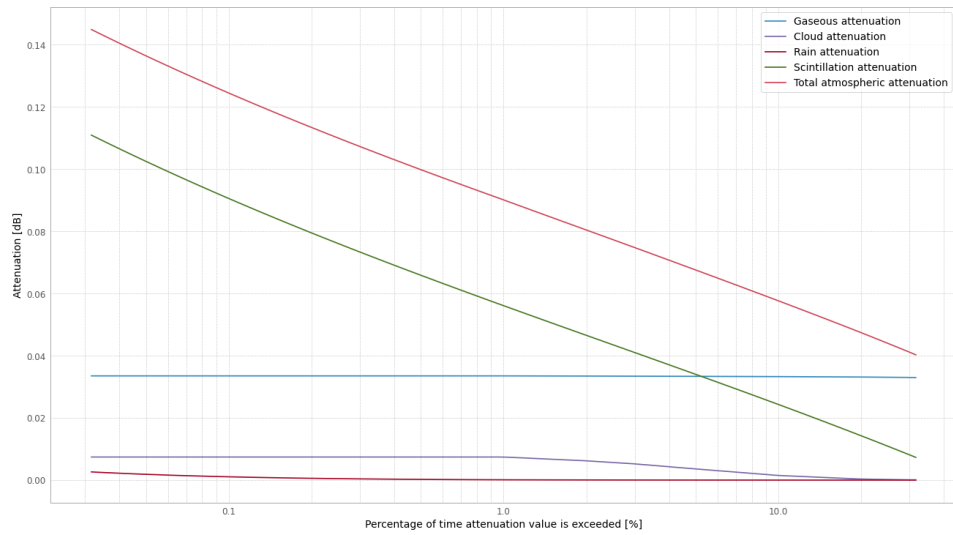


Fig. 39: Atmospheric Attenuation at certain frequencies

It can be seen that the attenuation is extremely small.

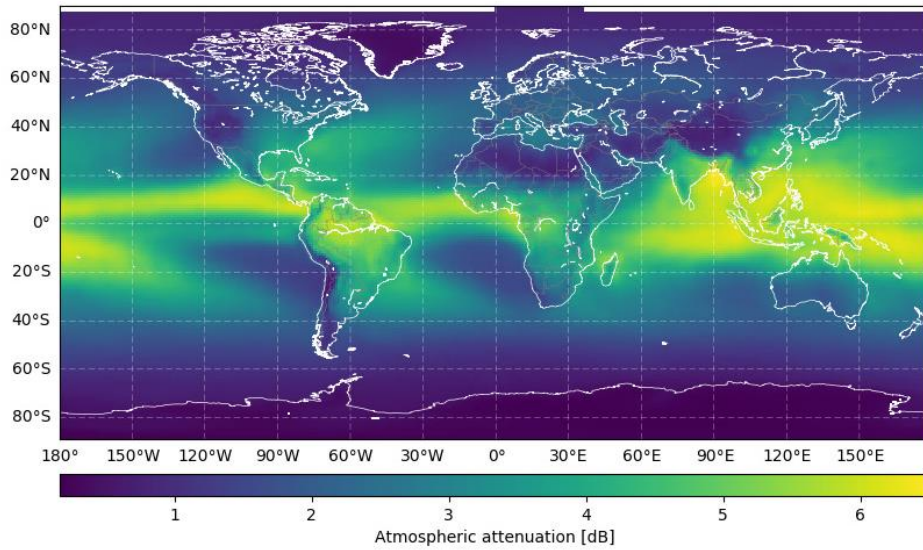


Fig. 40: Atmospheric Attenuation in India

Chapter 4

4.1 Hardware Setup

A block diagram of a professional observatory is shown below:

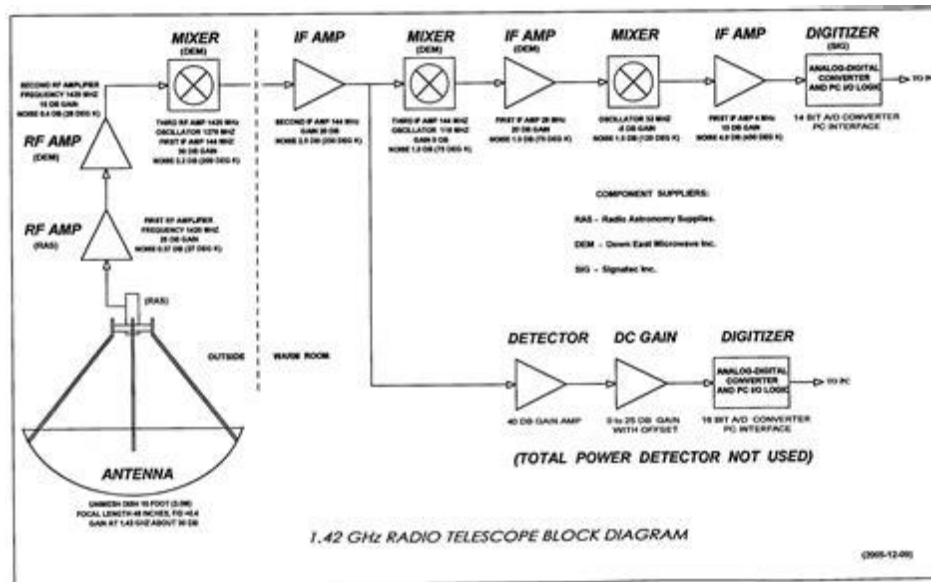


Fig. 41: Professional Observatory

A radio telescope is mainly broken down into three parts: the antenna, the receiver, and the radio system that converts it into readings suitable for a computer. We have designed the antenna above. The receiving system for a radio telescope, especially for one designed at 1.42GHz. The receiving system contains mixers, amplifiers, and filters, attenuators, and so on for signal conditioning. This is required when the observations have to be extremely precise. However, for our purposes, the hydrogen line is easily detected and does not require a large amount of signal conditioning.

The receiving system needs to be sensitive enough to detect the weak radio emissions from celestial sources. For this purpose, the main component of a receiving system is the signal amplifier. Because radio telescopes have to be extremely sensitive to small

signals, they are extremely sensitive to noise as well. Nowadays, modern electronics generate noise at 1420MHz as well. Therefore, it is essential to set up the radio telescope in an area where there isn't a lot of radio noise. A low-noise amplifier is connected to the feed probe. From there, the signal can either be transferred to a radio or be conditioned further. To detect nebulae and interstellar clouds, further filtering is required, but it is not necessary to detect objects like the Sun and the galactic centre.

The radio system that actually receives the signal and provides an audio-visual output can be many things. For extremely cheap systems, a satellite detector (insert photo here) is used. A satellite detector merely provides an audio output when your radio telescope picks up a signal. It does not provide output in usable and analysable forms. Therefore, amateur and professional setups use tools called software-defined radios.

Software-defined radios can roughly be defined as communication components that implement traditional radio components (such as mixers, filters, modulators, and so on) in an embedded system or by means of software on a personal computer. For example, a standard sound card operating on a personal computer can be used as a software-defined radio in order to detect solar flares. Signal processing is done on the computer's processing unit, instead of having specialized setups. The basic principle of operation is the principle of a super heterodyne receiver.

The principle of super heterodyne receiving is using frequency mixing in order to convert the original frequency to a frequency that is easier to analyse. A block diagram of a super heterodyne receiver is shown below:

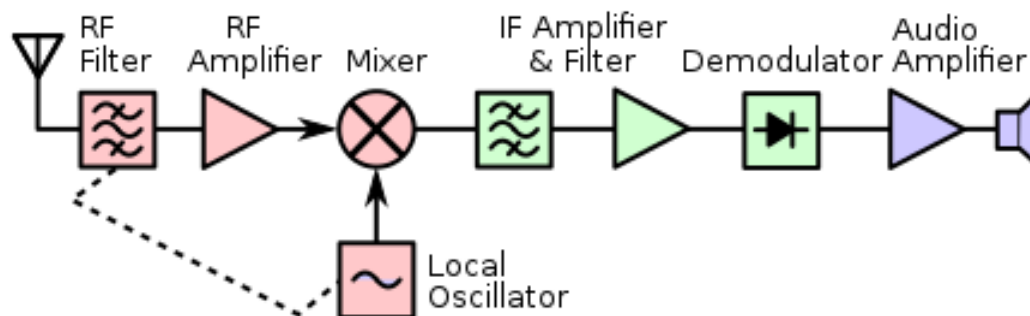


Fig. 42: Block Diagram of Super heterodyne Receiver

The radio signal is collected by the antenna. The tuned RF stage with optional RF amplifier provides some initial selectivity, which is required to suppress the picture frequency and may also prevent the first amplifier from being saturated by powerful out-of-passband signals. The mixing frequency is provided by a local oscillator, which is commonly a variable frequency oscillator that is used to tune the receiver to different stations. The real heterodyning is done by the frequency mixer, which converts the incoming radio frequency signal to a higher or lower, fixed, intermediate frequency (IF). The radio's amplification and narrowband filtering are mostly provided by the IF band-pass filter and amplifier. The audio or other modulation is extracted from the IF radio frequency by the demodulator, which is then amplified by an audio amplifier.

One of the major problems that arises in a super heterodyne receiver is called image frequency. The image frequency phenomenon occurs when a super heterodyne receiver automatically receives an input frequency mirrored about the desired frequency, due to its internal oscillations. This cannot be fully removed, but can be mitigated to a large extent by tuning the receiver correctly.

For our super heterodyne receiver, we have chosen the RTL-SDR. Specifically, our model is the RTL-SDR V3.



Fig. 43: RTL-SDR

The RTL-SDR is a dongle SDR with an SMA female input and a USB output. It is widely used and a large variety of software is compatible with the RTL-SDR. The block diagram of the RTL-SDR is shown:

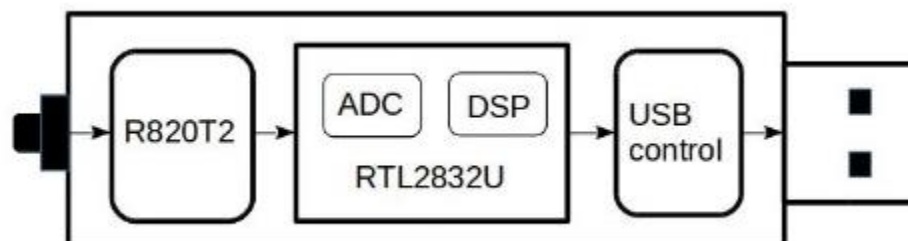


Fig. 44: Block Diagram of RTL-SDR

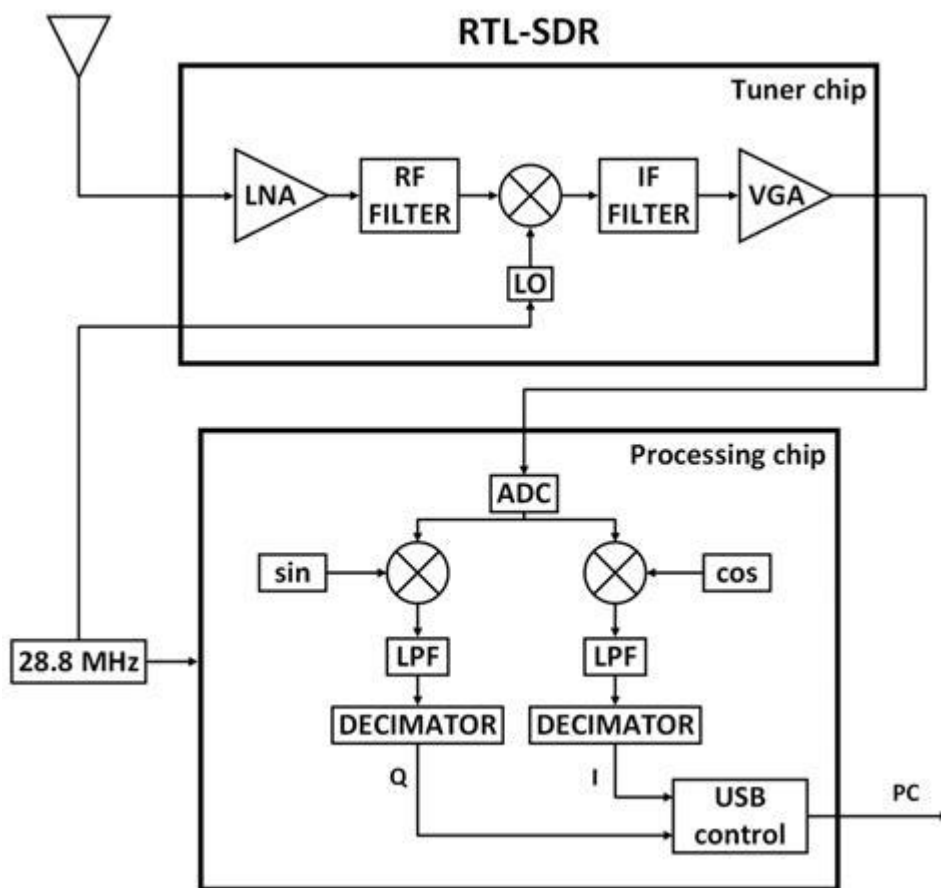


Fig. 45: Block Diagram of RTL-SDR

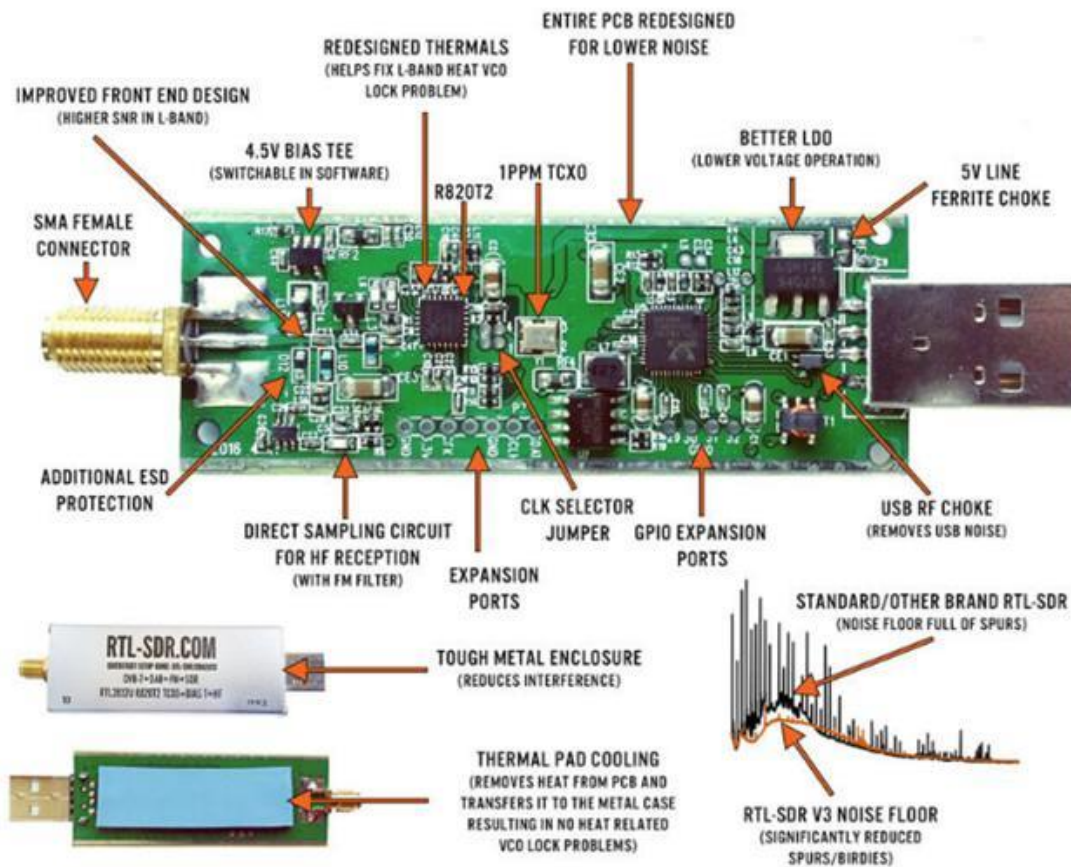


Fig. 46: Hardware Setup

Radio-frequency power amplifiers (RF amplifiers) typically convert low-power radio frequency (RF) signals to high-power RF signals. They are electronic devices that primarily use solid-state devices like MOSFETS to increase the power. They are primarily used to drive antenna receiving systems. They are the fundamental unit of receiving systems.

All components in a receiving system cause noise. Electronic circuits, in particular, produce noise called Gaussian noise. This type of noise is unavoidable and must be accounted for while processing. Amplifiers amplify not only the desired signal but also the noise. They also inject their own noise into the system. The amount of noise injected by cascading amplifiers can be derived using Friis' formula for noise:

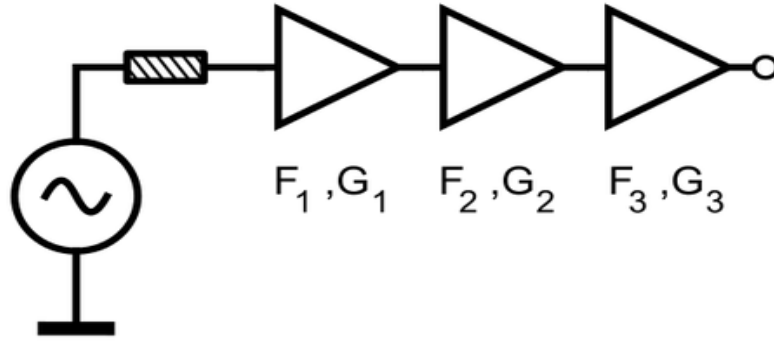


Fig. 47: Cascaded Amplifiers

Consider a system with amplifiers cascaded. The n^{th} amplifier has its own gain, G_n , and its own noise factor, F_n . The noise factor is simply $\frac{SNR_i}{SNR_o}$, the ratio of the input and output signal-to-noise ratios. These values are, in turn, the ratio of the incoming and outgoing powers. Friis' formula for cascaded noise assumes impedance matching, and hence the total noise factor is:

$$F_{total} = F_1 + \frac{F_2 - 1}{G_1} + \frac{F_3 - 1}{G_1 G_2} + \dots$$

For low-noise amplifying systems, this instantly shows us that:

$$F_{total} = F_{LNA} + \frac{F_{everythingelse} - 1}{G_{LNA}}$$

which leads us to the very important result:

The total noise of a radio receiver is largely determined by the first amplifier in the receiving chain.

For radio telescopes specifically, a special type of RF amplifier is required. This type of RF amplifier is called a low-noise amplifier (LNA). As the name suggests, these types of amplifiers are used to amplify very low strength signals from the background noise.

They are specially manufactured to have a very low noise figure, to provide the best output in Friis' formula. For our radio telescope, we use a wideband low-noise amplifier available Robu.

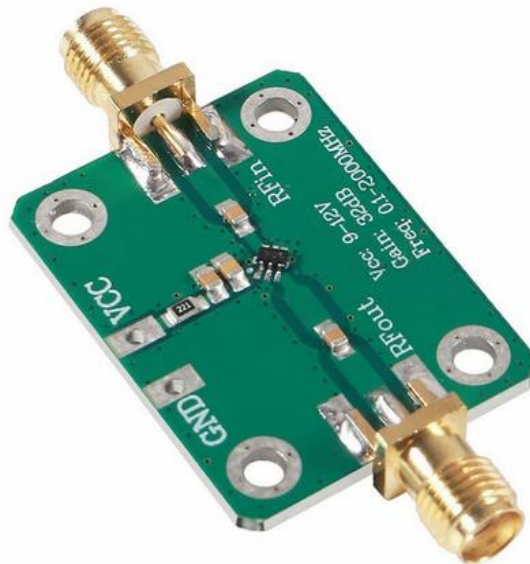


Fig. 48: RF Amplifier

The specifications of this amplifier are:

V_{cc}	9-12V
Gain at 1420 MHz	~26dB
Frequency range	0.1-2000MHz
Noise figure	4dB

Table 2: Specifications of RF Amplifier

This particular amplifier has an SMA female input and an SMA female output. It is powered by a rechargeable DC battery of rating 11.1V and 600mA. The power requirement of the amplifier is 1mW. This provides approximately 2 hours of continuous usage before the battery needs to be recharged.

The horn antenna itself is constructed out of 1mm thick aluminium. This is larger than the skin depth required, which is, as mentioned above, about 2-3 microns.

The 1mm aluminium sheets are welded together using oxyacetylene welding, and aluminium tape is used to provide electrical contact in between the edges in order to prevent loss due to the different impedance of the aluminium-oxyacetylene mixture. A hole of diameter 10mm is drilled in the waveguide at the top in order to allow the feed to create electrical contact to the horn, and the structure is held in place with electrical tape.



Fig. 49: Fabricated Horn Antenna

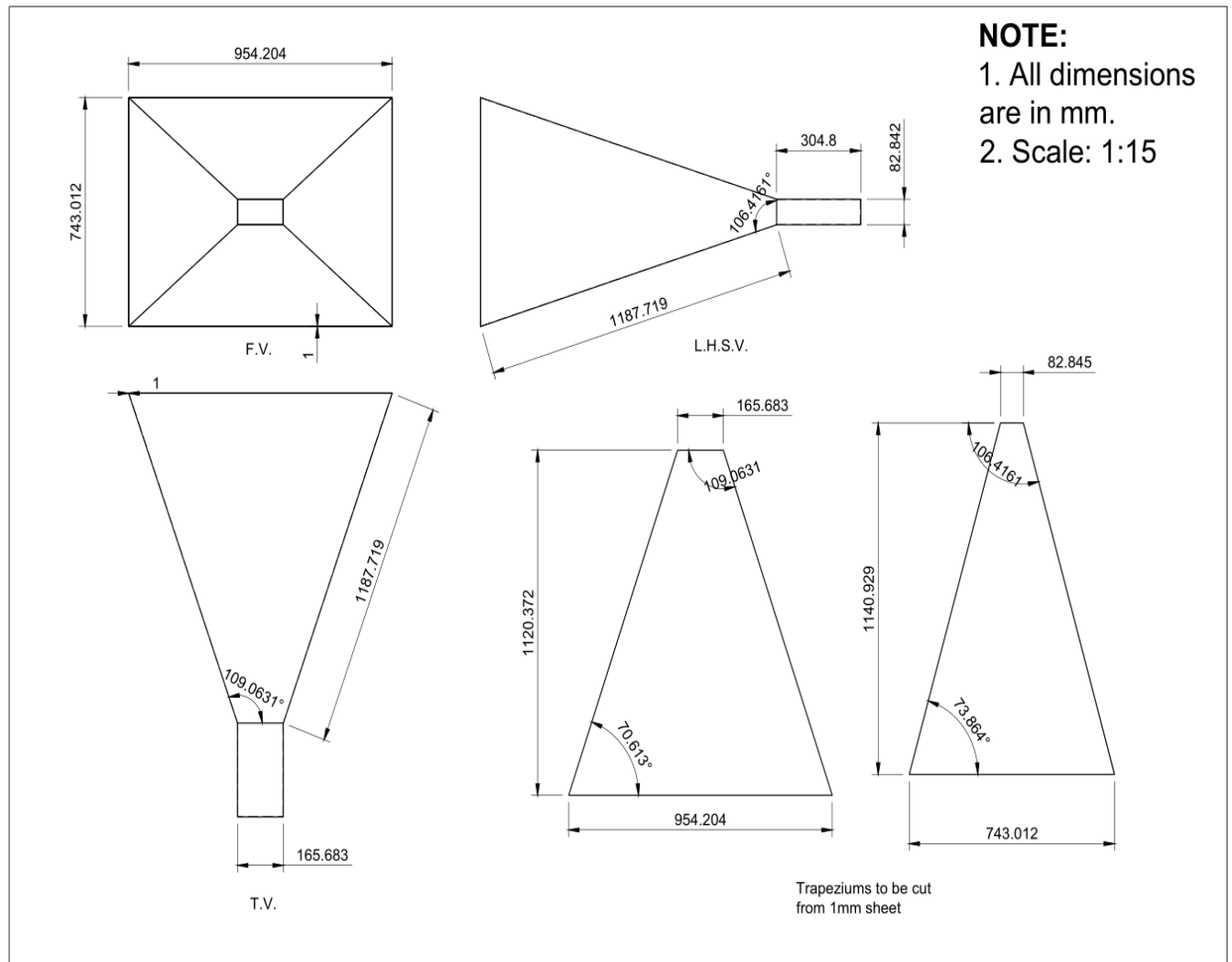


Fig. 50: CAED Model of Horn Antenna

The antenna feed consists of a brass rod approximately 1mm thick cut to the open-air quarter-wavelength of neutral hydrogen: 5.25cm . This is soldered to a type-N connector, which is attached to a Type-N to SMA connector. This connector directly feeds into the LNA, which is then attached through a short coaxial cable offering around 0.5dB loss to the RTL-SDR. The RTL-SDR is then attached through a USB port to a computer, where the data can be further analyzed.

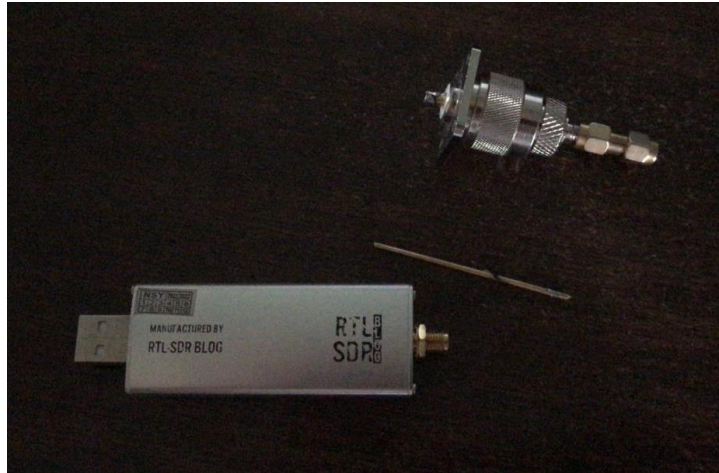


Fig. 51: Antenna Feed, Connector, RTL-SDR

The total cost of the setup is around Rs. 50000. Most of this cost comes in the welding and fabrication of the horn antenna, as well as the radio components which have to be imported. The coaxial cable reduces thermal noise in the system.

Chapter 5

5.1 Spectrometric Software Observations

GNU Radio is a free and open-source implementation of software-defined radios that runs in conjunction with many popular commercially-available SDRs. It can be used to create a simulation-like environment, or can be used with hardware. We used two spectrometers in order to receive and analyse radiation. The first spectrometer used was AirSpy's SDR Sharp with the IF average plugin.

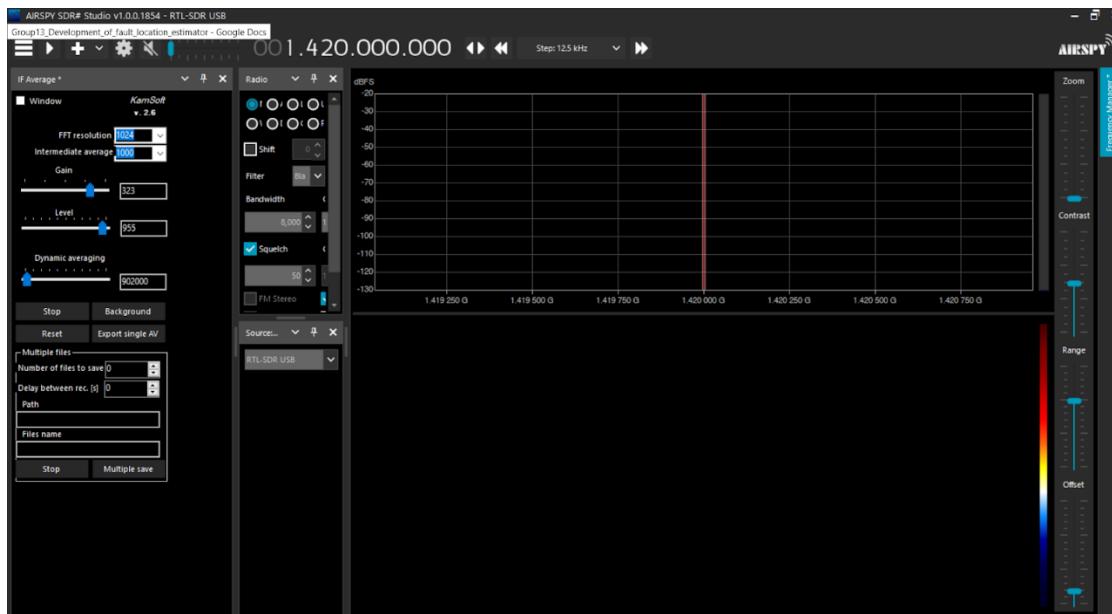


Fig. 52: 1.42 GHz observation in SDR Sharp

SDR Sharp is a spectrometer that provides real-time readings and can be adjusted to a wide range of frequencies. In fact, it is limited by the RTL-SDR's topmost frequency of operation, approximately 4.3GHz. The resolution of the SDR is 2.4MHz. To ensure our antenna was working, we first detected emission by CSAT, whose radio station operates at 1.44GHz.

This is close enough to 1.42GHz that the gain doesn't change all that much, due to the nature of the horn antenna.

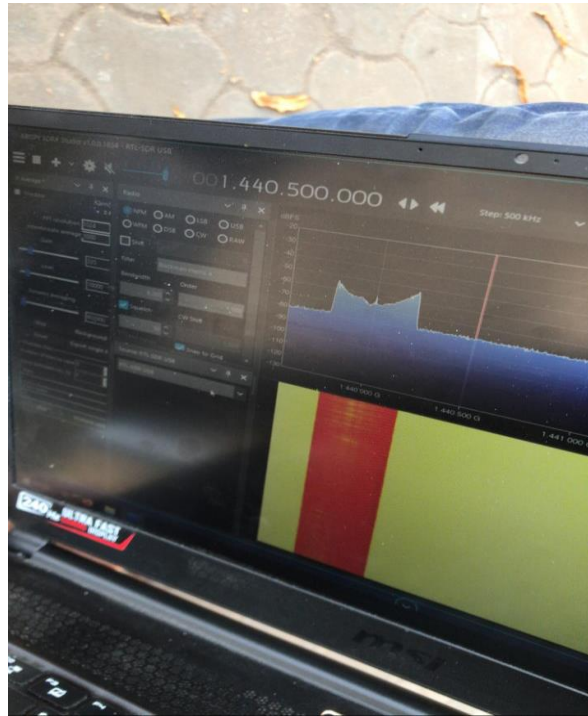


Fig. 53: 1.44 GHz observation in SDR Sharp

The observation is shown above. As shown, the basic noise floor is of -80dB. CSAT's radiation is detected at -60dB over a slightly wide band, which is what is expected to be observed. Thus we can conclude that our horn antenna provides roughly the simulated gain.

SDR Sharp was also used to detect the inherent noise generated by the SDR. At 1420MHz, three humps appear in the radio emission readings of the SDR. These are shown below:

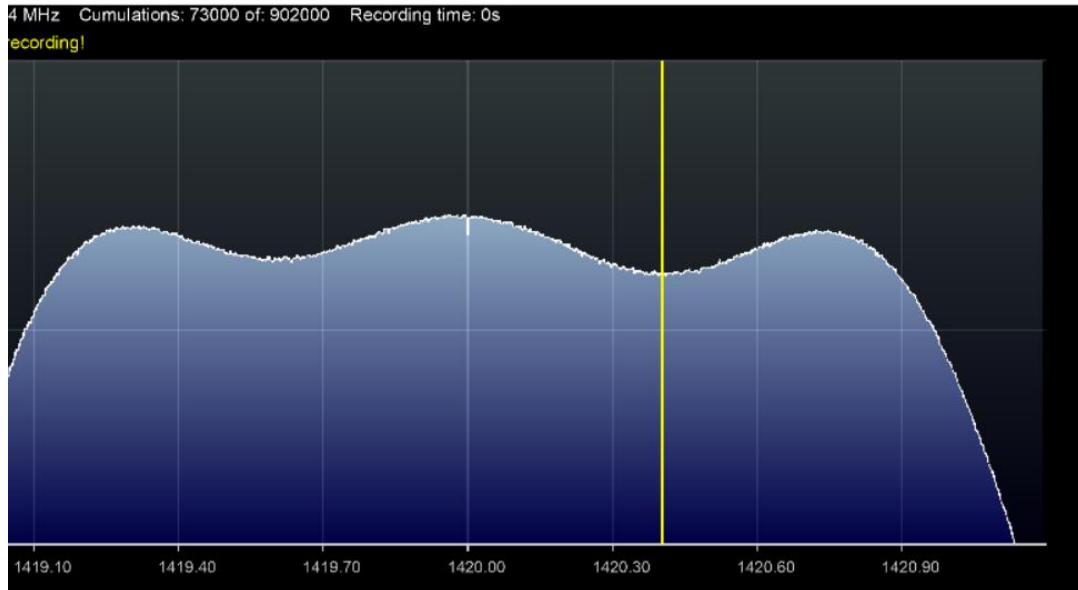


Fig. 54: Inherent Noise recorded on SDR Sharp

These are artefacts of the SDR and should not be mistaken for the hydrogen line, which appears in the same region. The hydrogen line is hidden in these three humps. The easiest way to remove these three humps is to perform background subtraction with SDR Sharp's inherent capabilities. SDR Sharp allows one to perform a cumulative average of the frequencies received, and subtract those frequencies from further observations. If we remove the background noise, then we can obtain the required signal. The way to do this is by calibrating SDR Sharp: let it record the background, averaging and all, and then let it subtract the background. To record the background, simply disconnect the antenna and wait for one cycle of the readings to finish.

The figure below shows the readings obtained by the horn antenna after background calibration when the antenna is *not* pointed towards any source.

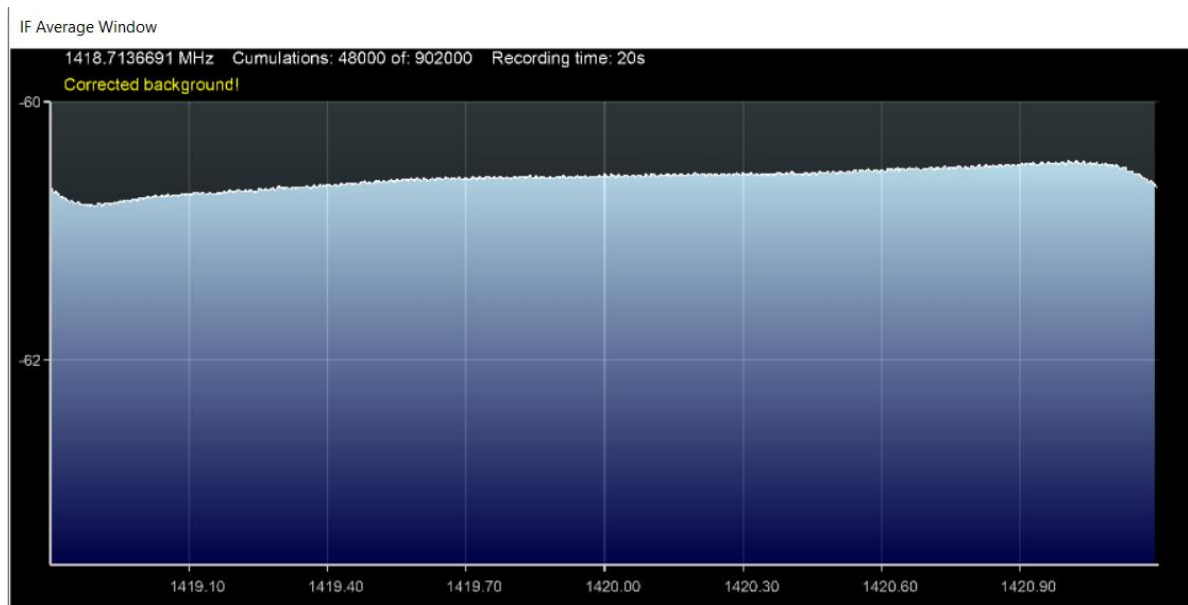


Fig. 55: Readings obtained by Horn Antenna when it is not pointed to any source

The figure below shows the readings obtained by the horn antenna after background calibration is performed and when the antenna is pointed towards a neutral hydrogen source.

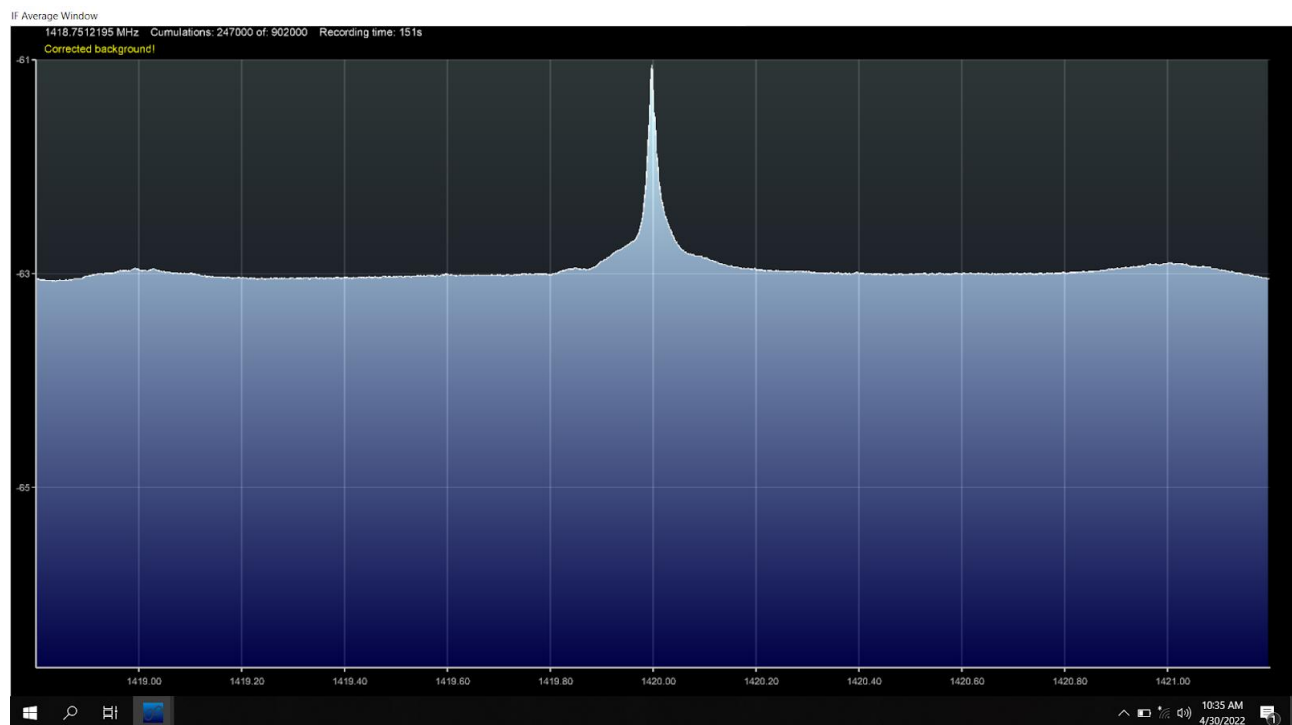


Fig. 56: Readings obtained by Horn Antenna when it is pointed to a source

Note that this reading is heavily exaggerated - the strength of the signal does not matter all that much in an SDR, merely the shape. One can observe some of the humps of the SDR left over in these readings, which the background calibration did not completely filter out. The central frequency is adjusted very slightly in order to bring the result to 1.42GHz. In reality, the actual value would be somewhere in between 1420.00 and 1420.80, depending on the object being observed. This particular observation is of the galactic centre, which is roughly stationary with respect to the solar system, hence there is not as much redshift as one would expect. It was performed at 10:35 AM on the 30th of April 2022.

5.2 Our implementation of a scaled down form of VIRGO

The VIRGO spectrometer is a spectrometer developed by Apostol's Spanakis-Misirlis written in Python that uses GNU Radio to perform observations. It is capable of performing a 4-type weighted-overlap add Fourier Transform, which reduces spectral side lobes at the cost of minimum computational increase in power. We created our own implementation of this in Python3 for reading the spectral data. While not as powerful or as versatile as the original VIRGO, it provides us with basic knowledge of how to create a spectrometer that works. The basic algorithm is outlined below:

The output signal in the k^{th} channel of the SDR can be represented as:

$$X_k(m) = \sum_{n=-\infty}^{\infty} h(mM - n)x(n)W_k^{-kn}$$

For $k = 0, 1, 2, 3, \dots, K - 1$

Here, the sample time m denotes the block number and the LHS is the short-time spectrum of the signal at time $n = mM$. Therefore, the discrete Fourier transform of the modified sequence $y_m(n) = h(mM - N)x(n)$

can be interpreted as this signal, such that

$$X_k(m) = \sum_{n=-\infty}^{\infty} y_m(n)W_k^{-kn} .$$

Here, $h(n)$ is the window sliding along the signal. Only on this part of the signal is the FFT performed. We define in order to set our origin at the beginning of the sliding window. After performing weighted-overlap addition using the Python package numpy, the results are plotted using matplotlib. We also created a tool for retrieving sample HI observations from the 2005 LAB survey of galactic hydrogen. The retrieval tool uses object names from the SIMBAD astronomical database. It uses the user's latitude and longitude in order to predict when the object will be up in the sky. A sample of those observations is given below:

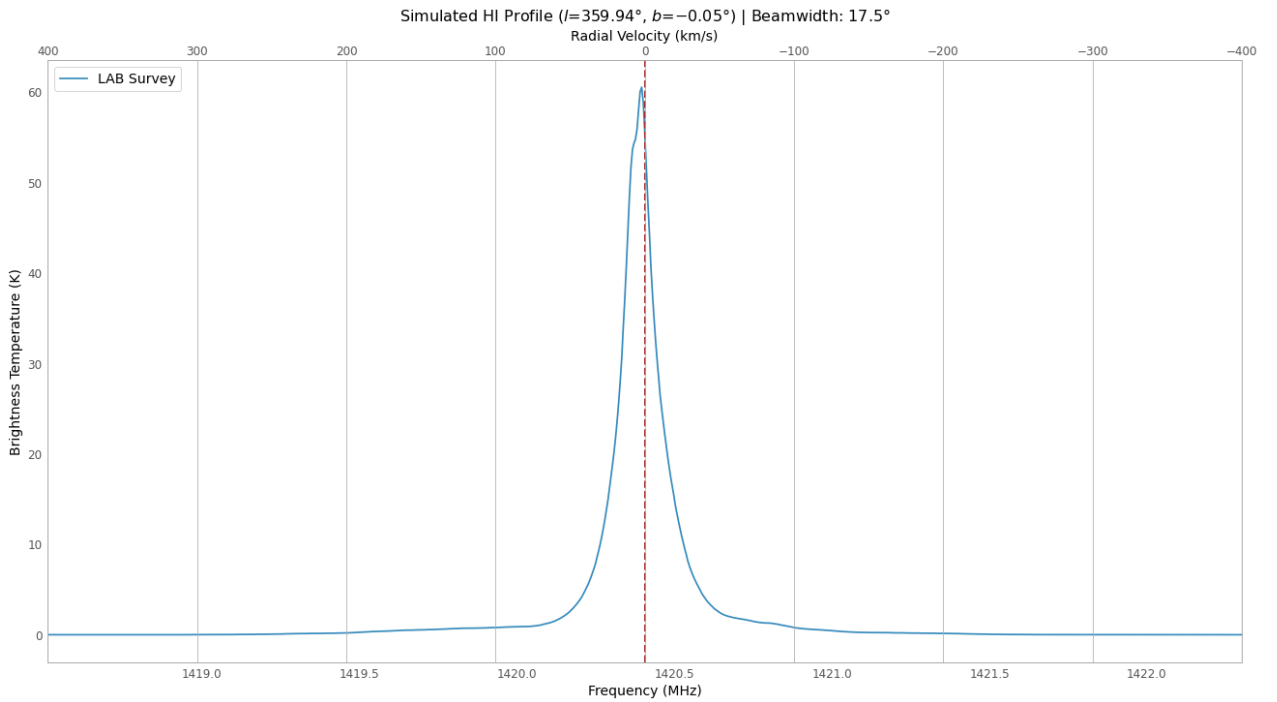


Fig. 57: Simulated HI Profile

A sample of the predictions is given below. Here, we predict the position of the centre of the galaxy (the supermassive black hole known as Sagittarius A*) on the 5th of April, 2022 as seen from Pune.

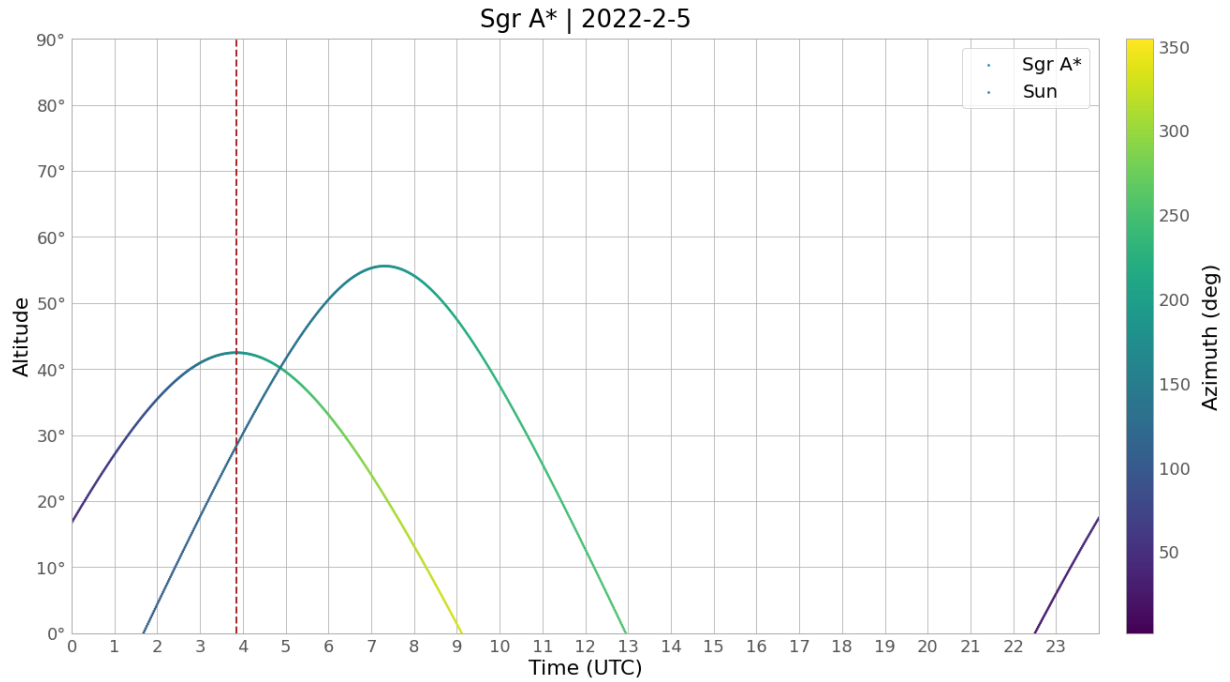


Fig. 58: Sample Prediction

It is seen that the prediction and simulation tools agree well with our observations of the galactic centre. Thus our horn antenna is functional.

5.3 Calculations

The final step is to calculate the galactic rotation curve. The theoretical setup is shown:

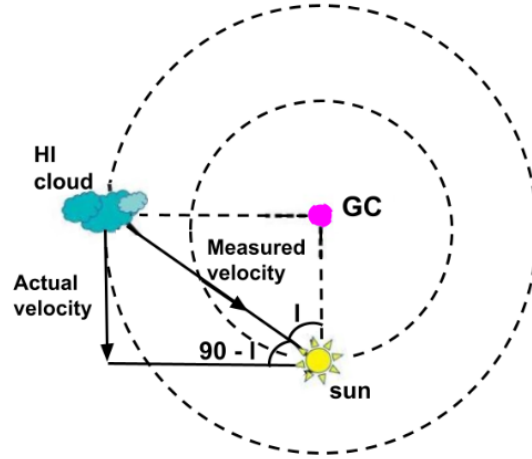


Fig. 59: Galactic Rotation Curve Setup

Here i is the inclination angle, measured from the galactic centre. The relative velocity can be given by:

$$V_r = \frac{V_{measured}}{\sin(90 - i)}$$

This is equivalent to saying $V_r = A d \sin(2l)$ where A is the Oort constant and l is the galactic longitude of the cloud or object being observed. Define w as the angular velocity at a certain point and w_0 as the angular velocity of the Sun around the galactic centre, to calculate the relative tangential velocity:

$V_t = (w - w_0)R_0 \cos(l) - dw$. Here R_0 is the distance from the galactic centre to the Sun (about 8.5kpc). We can rewrite this in terms of the Oort constants by $V_t = d(A \cos 2l + B)$. The radial velocity is: $U_r = V_r + V_0 \sin(l)$. The tangential velocity is $U_t = V_t + V_0 \cos l$, and the total velocity is simply the vector sum of these two.

We used the results from our observations with Virgo and the simulated results in order to derive the galactic rotation curve.

The galactic rotation curve is derived simply by assuming a perfectly circular orbit of the solar system around the galactic centre. This means that the centripetal force of attraction can be equated with Newton's law of gravity, to get the result:

$$V = \sqrt{\frac{GM}{R}}$$

The Doppler shift is given by:

$$f_{obs} = f_s \sqrt{\frac{1 - \frac{v}{c}}{1 + \frac{v}{c}}}$$

And therefore, we can approximate the galactic rotation curve. It will not be a full plot due to the lack of results, however we can plot the first few points:

S.No	Galactic Longitude in degrees	Galactic Latitude in degrees	Frequency in MHz	Relative velocity in km/s	Radial velocity in km/s	Tangential velocity in km/s	Distance in kpc	Total velocity in km/s
1	35	0	1420.40	-7.2	171.3	136.7	8.8	219.2
2	50	0	1420.40	-7.2	130.1	175.4	9.0	218.4
3	65	0	1420.40	-7.2	75.8	202.4	9.8	216.1
4	44	0	1420.45	-7.4	147.8	161.2	8.9	218.7

Table 3: Galactic Rotation Curve Data

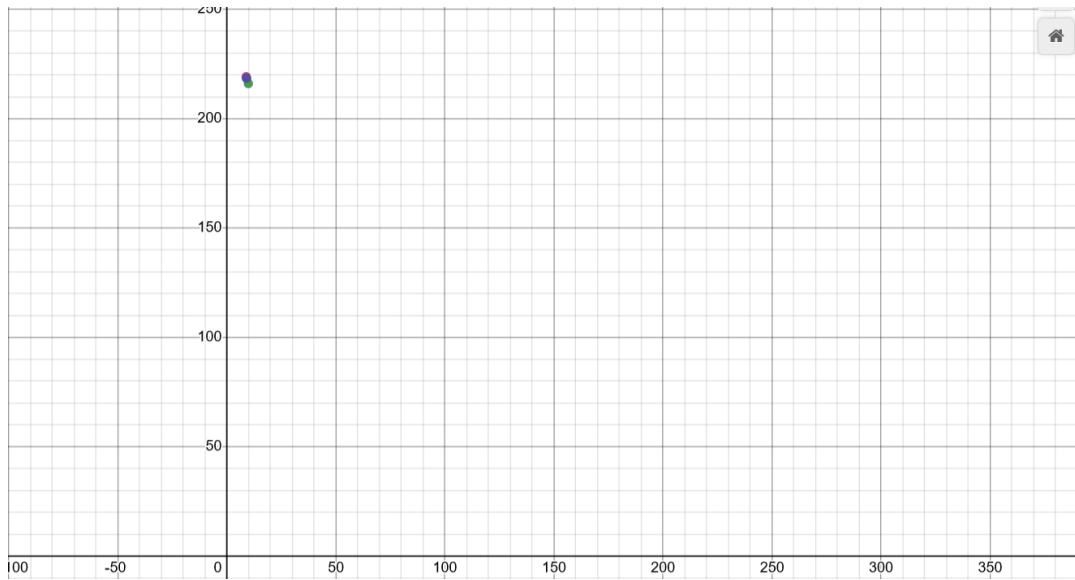


Fig. 60: Galactic Rotation Curve

With more points, the complete galactic rotation curve looks like this:

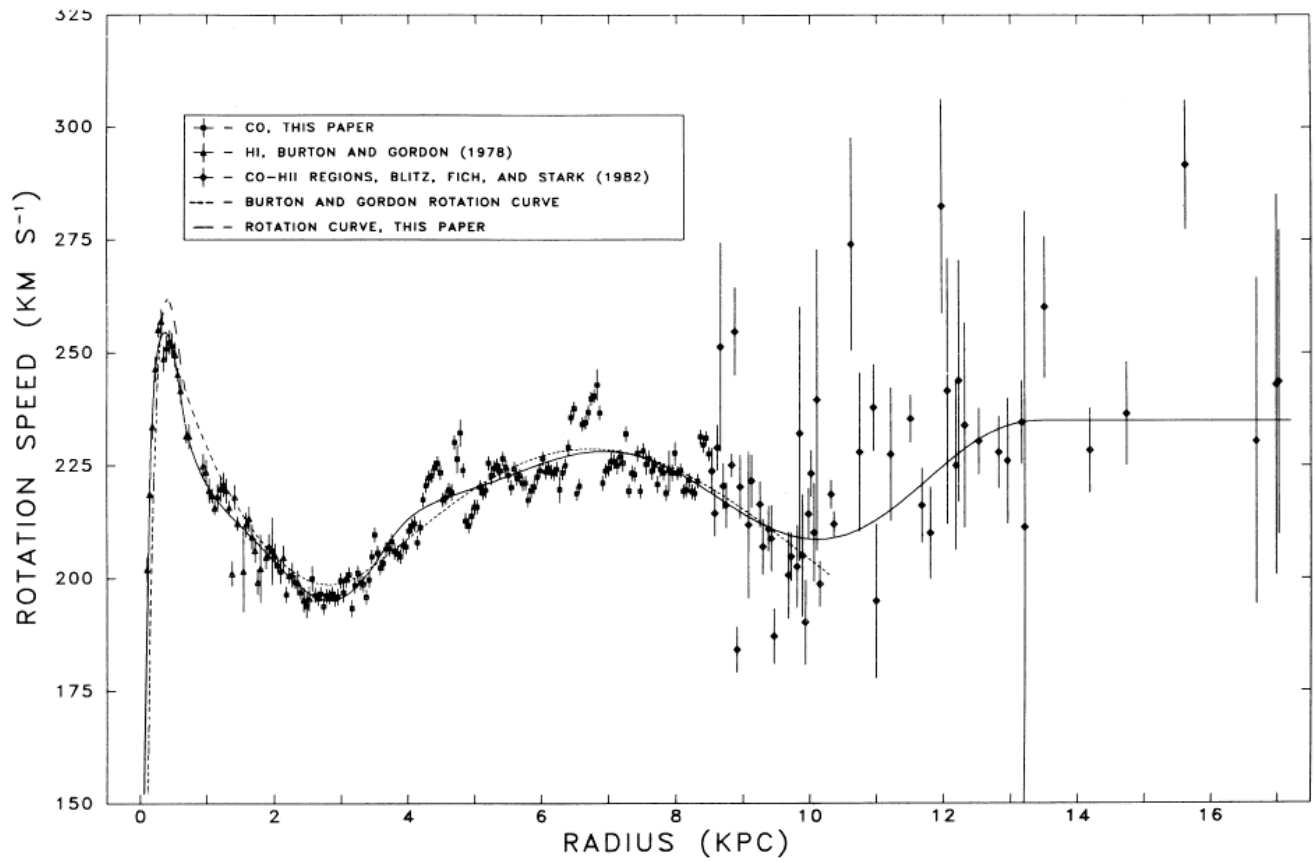


Fig. 61: Complete Galactic Rotation Curve

Chapter 6

6.1 Conclusion

We have constructed a relatively powerful small-scale radio telescope system that focuses on ease of use and instant results. We have also derived a very small part of the galactic rotation curve from it. With the use of off-the-shelf, readily available components, we have made it possible to detect sources of neutral hydrogen in our galaxy and derive fundamental astronomical results. The only custom component is a pyramidal horn antenna designed to accommodate internal reflection and a custom waveguide that has slightly better performance than commercial waveguides. The design of the horn antenna is presented in detail. We have completed the design and operated the radio telescope to observe Doppler shifts in the galaxy and thus calculated the relative velocities of objects moving relative to the solar system. The results are presented in a tabular form.

6.2 Future Scope

1. Automation of the radio telescope is the biggest improvement that can be made. Right now, operating the radio telescope is difficult because of the manual labour required to point it at different positions. Automation that allows it to point to any position in the sky is needed.
2. Better signal conditioning to pick up different sources is required. Adding band pass filters, multistage amplifiers, and fully utilizing the power of the VIRGO spectrometer can all provide marked improvements to the telescope.
3. Construction of an interferometric array is possible to gain even better results.

6.3 Challenges

1. Temperature control systems are required for the operation of a radio telescope for extended periods of time. This is because all components overheat and the system is susceptible to thermal noise, especially when operated in India.
2. Observations must be taken at awkward times, and remote systems need to be installed to comfortably record these observations. This is because the Milky Way is generally only visible during the very early hours of the day.
3. Gaussian noise from CSAT's radio station must be accounted for while attempting to fine-tune the observations taken.

Bibliography

1. *The Feynman Lectures on Physics*, Book III, Chapter 12
2. Griffiths, D. J. (1982). "Hyperfine Splitting in the Ground State of Hydrogen". *American Journal of Physics*. **50** (8): 698–703.
3. Francis, Charles; Anderson, Erik (June 2014). "Two estimates of the distance to the Galactic Center". *Monthly Notices of the Royal Astronomical Society*. **441** (2): 1105–1114
4. Robert E Collins, *Antennas and Radiowave Propagation*
5. Pandian B et al, *Galaxy Rotation Curve Measurements with a low-cost 21 cm Radio Telescope*
6. Dustin Johnson, Alan Rogers, *Development of a new generation Small Radio Telescope*
7. Nimish Patel, Rishi N Patel, et al, *A Low-cost 21 cm Horn-antenna Radio Telescope for Education and Outreach*, American Astronomical Society Meeting Abstracts, Volume 224
8. E. Smith, E. White, G. Langston and R. Prestage, "Open Source Radio Telescopes: Astronomy Projects for Students, Teachers, and Amateurs," 2018 2nd URSI Atlantic Radio Science Meeting (AT-RASC), 2018, pp. 1-3, doi: 10.23919/URSI-AT-RASC.2018.8471331.
9. K. Bandura, R. Prestage and P. Sanghavi, "The Digital Signal Processing in Radio Astronomy (DSPIRA) Program," 2018 2nd URSI Atlantic Radio Science Meeting (AT-RASC), 2018, pp. 1-1, doi: 10.23919/URSI-AT-RASC.2018.8471474.
10. <https://wvurail.org/lightwork/memos/LightWorkMemo022-r13.pdf>
11. Natalia Nikolova, *Antenna Engineering*
12. Pereira et al, *New Method for Optimum Design of Pyramidal Horn Antennas*, *Journal of Microwaves, Optoelectronics and Electromagnetic Applications*, Vol. 10, No. 1, June 2011

13. <https://www.everythingrf.com/tech-resources/waveguides-sizes>)
14. Wade, P. (2006). *Rectangular Waveguide to Coax Transition Design*. W1GHZ
15. Banjeglav, G., & Malarić, K. (2015). *2.4 GHz horn antenna*. Transactions on maritime science, 4(01), 35-40.
16. Pozar, D. M. (2011). *Microwave engineering*. John Wiley & Sons.
17. Inigo del Portillo, *ITU-Rpy: A python implementation of the ITU-R P. Recommendations to compute atmospheric attenuation in slant and horizontal paths*, Github
18. Spanakis-Misirlis et al., (2021). *Virgo: A Versatile Spectrometer for Radio Astronomy*. Journal of Open Source Software, 6(62), 3067, <https://doi.org/10.21105/joss.03067>

Acknowledgments

With all respect and gratitude, we would like to thank all the people who have helped us directly or indirectly for this project work.

We express our hearty gratitude and sincere thanks to **Prof. Dr. S. S. Dambhare, Head of Department (Electrical Engineering)**.

We pay our deep sense of gratitude to **Dr, Archana G. Thosar** our **Guide** and for her valuable guidance and kind supervision throughout the course to complete the project work on **“Design of an Automated Radio Telescope for observing the 21 cm Hydrogen Line.”**

We feel to acknowledge our indebtedness, deep sense of gratitude and sincere thanks to all teaching and non – teaching staff members of the department for their valuable ideas, guidance, kind supervision, encouragement and for providing necessary information and required resources timely during each stage of the project work.

We are ending this acknowledgement with deep indebtedness to our friends, family and each and every person who has helped us directly or indirectly to complete the manuscript.

Thank you!

1. Kshitij Duraphe
2. Revati Bhangale
3. Tanaya Wankhede
4. Divya Singh

Appendix

Observations can be scheduled using Stellarium, a software that accurately simulates the sky and stellar positions from any location on Earth. It is useful for planning observations because it tells you the exact positions of interesting objects. An image of Stellarium's user interface is shown below:



Fig. 62: Stellarium's User Interface

At the particular moment this image was simulating, the Sun was setting in the West while the curve of the Milky Way enveloped it. Ordinarily, it is difficult to detect the hydrogen line because of the interference caused by the Sun, which itself does not emit very strongly at neutral hydrogen.

Stellarium is open-source and extensible, allowing it to interface with GNU Radio and VIRGO. We have used GNU Radio's inbuilt capability to interface with Stellarium to draw the prediction graph.